Author:	Gan, Zhixing; Wen, Xiaoming ; Chen, Weijian ; Zhou, Chunhua; Yang, Shuang; Cao, Guiyuan; Ghiggino, Kenneth P.; Zhang, Hua; Jia, Baohua
Title:	The dominant energy transport pathway in Halide Perovskites: Photon recycling or carrier diffusion?
Article number:	1900185
Year:	2019
Journal:	Advanced Energy Materials
Volume:	9
Issue:	20
URL:	http://hdl.handle.net/1959.3/448783
Copyright:	Copyright © 2019 WILEY-VCH Verlag GmbH & Co. KGaA, Weinheim.This is the peer reviewed version of the following article: Gan, Z. X., Wen, X. M., Chen, W. J., Zhou, C. H., Yang, S., Cao, G., Ghiggino, K. P., Zhang, H., Jia, B. H., The Dominant Energy Transport Pathway in Halide Perovskites: Photon Recycling or Carrier Diffusion?. Adv. Energy Mater. 2019, 9, 1900185., which has been published in final form at https://doi.org/10.1002/aenm.201900185. This article may be used for non-commercial purposes in accordance with Wiley Terms and Conditions for Use of Self-Archived Versions.

The definitive version is available at: https://doi.org/10.1002/aenm.201900185

The Dominant Energy Transport Pathway in Halide Perovskites: Photon Recycling or Carrier Diffusion?

Zhixing Gan, Xiaoming Wen, Weijian Chen, Chunhua Zhou, Shuang Yang, Guiyuan Cao, Kenneth P. Ghiggino, Hua Zhang and Baohua Jia**

Dr. Z. X. Gan, Dr. X. M. Wen, Dr. W. J. Chen, C. H. Zhou, B. H. Jia,
Centre for Micro-Photonics, Swinburne University of Technology, Hawthorn 3122, Australia
E-mail: xwen@swin.edu.au; bjia@swin.edu.au

Dr. Z. X. Gan,
Key Laboratory of Optoelectronic Technology of Jiangsu Province, School of Physics and Technology, Nanjing Normal University, Nanjing 210023, China

Dr. S. Yang, Prof. H. Zhang,
Center for Programmable Materials, School of Materials Science and Engineering, Nanyang Technological University, 50 Nanyang Avenue, Singapore 639798, Singapore

Prof. K. P. Ghiggino,
School of Chemistry and ARC Centre of Excellence in Exciton Science, University of Melbourne, Parkville, VIC, 3010 Australia

Keywords: halide perovskites, photon recycling, carrier diffusion, photoluminescence

Photon recycling and carrier diffusion are the two plausible processes that primarily affect the carrier dynamics in halide perovskites, and therefore the evaluation of the performance of their photovoltaic and photonic devices. However, it is still challenging to isolate their individual contributions because both processes result in a similar emission redshift. Herein, we confirm that photon recycling is the dominant effect responsible for the observed redshifted emission. By applying one- and two-photon confocal emission microscopy on Ruddlesden−Popper type two-dimensional (2D) perovskites, of which inter-plane carrier diffusion is strictly supressed, the substantial PL redshift (72 meV) is well reproduced by the photon transport model. A comparison of 3D bulk $CH_3NH_3PbBr_3$ single crystal to 2D perovskite by depth resolved two-photon PL spectra reveals the contribution of carrier diffusion on energy transport at a distance beyond diffusion length is constantly negligible, though the carrier diffusion indeed exists in the 3D crystal. Our investigation resolves the fundamental confusion and debate surrounding

the issue and provides significant insights into carrier kinetics in perovskites, which is important for future developments in solar cells and other optoelectronic devices.

1. Introduction

The emerging lead halide perovskites have attracted enormous attention due to their excellent performance in optoelectronic applications, such as solar cells,1-7 light emitting devices (LEDs),[8-10] photodetectors,[11-13] and lasers.[14-17] Regarding the solar cells, the diffusion of photogenerated carriers and photon recycling are the two possible energy transport pathways that could affect the internal carrier dynamics and device performances.[18-21] Both processes may cause a similar influence in the external emission wavelength. Whereas, their influences on carrier lifetime, external photoluminescence (PL) quantum yield (QY), as well as open-circuit voltage (V_{OC}) and efficiency of the solar cells are different.[18,19] Photon recycling refers to the regeneration of an excitation via the self-reabsorption of emission from recombining photo-generated charge pairs.[18] For solar cells, generally, the performance can be boosted by a highly efficient photon recycling process.[18-21] As demonstrated previously, photon-recycling will boost an additional open-circuit voltage (ΔV_{OC}^{PR}) according to,[20] $q\Delta V_{OC}^{PR} = kT_C \ln(\frac{1}{1-p_r\eta_{IN}})$, where k is the Boltzmann constant, q is the elementary charge of an electron, T_C is the cell temperature, η_{IN} is the internal quantum efficiency, and p_r is the probability of photon recycling. On the other hand, for LEDs, strong photon recycling implies a low out-coupling probability (η_{esc}), which is detrimental for external efficiency. For example, an internal PL QY lower than 95% can result in an external PL QY lower than 50%.[18] Moreover the photophysics behind photon recycling and carrier diffusion are different. The high photon recycling efficiency generally requires a large overlapping of its PL spectrum with the absorption spectrum, a strong photon confinement, and a high-internal PL quantum yield.[18-20] While long carrier diffusion length is ensured by long carrier lifetime, high carrier mobility, and low defect density.[22-27] These two energy transport pathways imply different applications, therefore, it is crucial to evaluate the contributions of photon recycling and carrier diffusion in lead halide perovskites.

In perovskites, very long diffusion lengths exceeding one micron in solution-fabricated films and hundreds of microns in single crystals have been reported,[22-27] enabling the radiative recombination of charge carriers at positions far away from the excitation spot. On the other hand, due to the highly efficient band-to-band transitions, large absorption coefficients, and small luminescence Stokes-shifts,[27-30] the recycling possibility of luminescence photons is also quite high.[18,19,30-38] Consequently, there has been a fierce debate whether carrier diffusion or photon recycling, dominates the energy transport and internal recombination processes in perovskites.[18,19,39-41] Friend's group has claimed that photon recycling plays a pivotal role on power conversion efficiencies for both LEDs and solar cells.[18,19] On the other hand, Huang's group suggested the role of photon recycling is minor, highlighting the intrinsically long carrier recombination lifetime instead of the photon-recycling-induced photon propagation as the origin of their long carrier diffusion length.[39-41]

This debate was frequently investigated by the PL variation as a function of separation of excitation and emission position.[19,42,43] In these experiments, the excitation spot and emission collection position are different, thereby allowing photo-generated carriers or emission photons to travel internally before measurements. For example, when the excitation beam is irradiated on the front of a perovskite crystal, the PL emission spectra collected from the front and from the rear of the crystal are different, which is explained by the pure photon reabsorption process.[42] Tian et al measured individual single-crystal $MAPbI_3$ ($MA=CH_3NH_3$) and $MAPbBr_3$ nanowires (NWs) and nanoplates (NPs) using PL-scanned imaging microscopy with a galvano-mirror.[43] The excitation laser spot was parked in a specific position of the NWs and NPs, and the PL signal collection spot was changed over the entire sample by rotating the galvano-mirror. Through monitoring the time-resolved PL at different collection spots, carrier diffusion coefficient, charge mobility, recombination rate constants, and carrier diffusion length were determined based on a carrier diffusion model completely neglecting the photon recycling effect. Besides these two contrary explanations, in many other reports, both carrier diffusion and photon recycling are ambiguously included.[19,30,32-34] These reports claim that energy transport is not limited by diffusive charge transport but can occur over long distances through multiple re-absorption-diffusion emission events implying the repeated recycling between photons and electron-hole pairs.[19] In addition, the same physical effects were also intensively studied by the excitation depth dependent PL or cathode-luminescence and PL of perovskite with different thickness.[30-33] Very similar redshifts of the PL maximum were consistently observed.[30-33] Unfortunately, to date, conclusions based on the same observation are often conflicting, leading to an unresolved puzzle.[18,19,30-43]

This controversy commonly exists in various perovskites and device studies. The confusion on this issue makes the photocarrier dynamics unclear and misestimation of conversion efficiency of perovskite based solar cells,[4,44] affecting the understanding of practical devices such as solar cells and LEDs. In particular, the long carrier diffusion length is regarded as a crucial parameter leading to the advanced photovoltaic properties of perovskite-based solar cells. However, misunderstandings may lead to incorrect insights, for example, the underestimation of photon recycling will result in an incorrect measurement of the intrinsic carrier diffusion parameters and internal recombination coefficients.

2. Results

2.1 Thickness dependent photoluminescence of 2D perovskite platelets

As shown in **Figure 1**a, in the carrier diffusion model, the excited carriers are generated at the excitation spot and then diffuse to other sites along the carrier gradient before radiative recombination.[19,30,32-34] A portion of the photogenerated electrons and holes may reach the PL collection site and recombine. During the diffusion, the excited carriers may lose a small amount of energy, resulting in a redshift of emission. While in the photon recycling model (Figure 1b), fluorescence photons are firstly emitted by the carrier recombination at the excitation spot and then propagate inside the perovskite.[18,19,30-34] The photon reabsorption-emission repeats over a long propagation distance, resulting in a reduced PL photon energy and intensity. It is worth noting the photon reabsorption without reemission, also known as inner filtering, should be distinguished from the photon recycling effect,[39] see discussion in Figure S1, Supporting Information (SI). Both carrier diffusion and photon recycling can occur in perovskite, but normally they lead to similar red-shifts in peak position, suggesting it is a formidable challenge to distinguish between these two photophysical processes, and to quantify the contribution of each effect.

To address this challenge, a two dimensional (2D) perovskite $(BA)_2PbI_4$ ($BA=CH_3(CH_2)_3NH_3$) single crystal is investigated here using combinations of thickness/depth dependent steady state PL and time-resolved PL (TRPL) on confocal microscopy measurements. The Ruddlesden−Popper type 2D perovskites consist of well-defined inorganic perovskite layers intercalated with bulky butylammonium (BA) cations acting as spacers between these fragments (Figure 1c).[45-49] Structural characterization of the $(BA)_2PbI_4$, including transmission electron microscopic (TEM) images, selected electron diffraction, X-ray diffraction (XRD) pattern, and optical microscopy images can be found in Figure S2-4, SI. In this special multi-quantum-well structure, the carriers are therefore tightly confined in the 2D inorganic layers.[50] The excitons feature large binding energies and fast recombination within the quantum-well, as validated previously.[51] It suggests the diffusion of photogenerated carriers in the direction perpendicular to the 2D plane is highly suppressed (Figure S5, SI). A confocal microscope set-up depicted in Figure 1d is used for measuring the PL spectra and TRPL decay in the transmission configuration, in which the excitation beam is perpendicular to the perovskite samples with various thicknesses and only emission at the focussed spot is collected by the detector via the objective due to the spatial selection of the confocal microscope. The two objectives are independently controlled to ensure the transmitted PL is largely acquired. Further details of the instrument setup can be found in Figure S6, SI. For such sample and detection design, the off-axis emission originating from carrier diffusion is negligible because of the filtering effect of the defocus signals by the confocal pinhole.

The 2D perovskite platelets with different thicknesses (d) were fabricated by a mechanical exfoliation method and then selected by atomic force microscopy (AFM). Typical AFM images and corresponding PL spectra are shown in **Figure 2**a-f. All the exfoliated 2D perovskites are flat platelets with lateral sizes from several to tens of microns. When the thickness is about 51 nm, the PL peak appears at around 521.6 nm, with symmetric spectral shape, which can be well fitted by a Gaussian function (Figure 2g). As the thickness increases, a redshift in the PL peak wavelength is observed. The PL peak moves to 527.8 nm when the thickness is approximately 2.2 μm (Figure 2c,f). When the thickness increases to 30 μm and even bulk of 396 μm, further redshifted emission still can be observed. In addition, the profile of the PL spectrum becomes asymmetric. This observation is very similar to previous reports on 3D type perovskites (Table

S1, SI),[19,30,31] implying our following conclusion is generally applicable. The quantum confinement caused PL redshift is excluded here because it has only been demonstrated in 2D perovskite materials with limited monolayers.[46] While in our case, 2D perovskite materials with a large layer number are employed. As plotted in Figure 2h, the PL peak would continuously redshift to 538 nm with further increase of the thickness to ~396 μm (a bulk crystal).

The absorption spectrum shown in **Figure 3**a is characteristic of direct bandgap excitation with a strong absorption above the band edge. The absorption coefficient (α_λ) is up to 10^4 cm^{-1}, which rapidly decreases when the photon energy is below the excitonic transition. Based on the absorption coefficient, the effect of reabsorption through the thickness of the 2D platelet was calculated using the Beer–Lambert reabsorption model.[19,30,42]

$$I(\lambda, d) = I_0(\lambda)\exp(-\alpha_\lambda d). \quad (1)$$

where $I_0(\lambda)$ is the initial emission spectrum without reabsorption, λ is wavelength, and d is thickness. Herein, the Gaussian function fitted in Figure 2g is approximately regarded as $I_0(\lambda)$. The calculated PL spectra at different thicknesses are presented in Figure 3b. The emission spectra continuously red-shift and become asymmetric as the thickness increases, which is in good agreement with the experimental results. The dependences of the PL peak position on thickness are plotted in Figure 3c from both experimental and calculated results. The coincident relationships confirm that the observed PL redshift is mainly caused by the photon transport without carrier diffusion. Moreover, the photon recycling was further evidenced by PL measurements based on reflection mode (Figure S7, SI). And the existence of photon transport within the perovskites is directly visualized by waveguiding effects (Figure S8, SI).

When the thickness is about 30 μm, a comparison of the experimental and calculated PL spectra is shown in Figure 3d. Although the peak positions are the same, the spectral shapes show some discrepancies. In detail, the experimental spectrum matches well with the calculated one in the high energy range (500-530 nm), while the experimental spectrum shows a higher long tail extending to 600 nm. This inconsistency is likely caused by re-emission of photon recycling, which is not considered in the Beer-Lambert predictions. As discussed in Figure S1, SI, the experimentally collected emission includes both the filtered photons and recycled photons.

The PL kinetics without photon recycling can be simply described by the following rate equation:[19,51]

$$\frac{\mathrm{d}n}{\mathrm{d}t} = G - k_1 n - k_2 n \qquad (2)$$

where n is the carrier density and t is time, G is the generation rate of the charge density, and the $k_1 n$, $k_2 n$ terms represent defect trapping (Shockley−Read−Hall recombination) and exciton recombination, respectively.[52] The radiative recombination of photogenerated carriers in multi-quantum-wells structure 2D perovskites is dominated by excitons, thus it is a first-order term.[47,50] Due to the low Auger coefficient[51] and the low excitation power density used (0.375 W/cm^2), here Auger recombination is negligible. When considering photon recycling, a photon density term γ_λ is added.[19]

$$\frac{\mathrm{d}n}{\mathrm{d}t} = G + \frac{c}{n_s}\Sigma\alpha_\lambda\gamma_\lambda - k_1 n - k_2 n \qquad (3)$$

where c is the speed of light, n_s is the refractive index (Figure S9, SI). γ_λ is described as,

$$\frac{\mathrm{d}\gamma_\lambda}{\mathrm{d}t} = k_2 n P_{stay} P_\lambda - \frac{c}{n_s}\alpha_\lambda\gamma_\lambda \qquad (4)$$

in which P_{stay} is the probability of the photon staying in the platelets, and P_λ is the probability that light will be emitted with a given wavelength. According to these equations, the photon-recycling process generates additional carriers leading to a measured PL lifetime longer than the intrinsic lifetime, which has been verified previously.[30,31,53,54]

2.2 Depth dependent two-photon photoluminescence of 2D perovskite crystal

In order to obtain more robust support from carrier lifetime, the depth dependent two-photon-excitation PL (TPL) measurements are conducted, by using 960 nm femtosecond laser.[55] Since the two-photon absorption and thus TPL intensity is proportional to the square of instantaneous excitation intensity, the photocarriers are selectively excited at the focal point, where the excitation intensity is high enough,[30-32,34,55,56] implying the TPL signal can be collected at a high temporal and spatial resolution.[56] More details of the setup can be found in Figure S6, SI. As depicted in the inset of **Figure 4**a, by changing the focal plane of the excitation laser (960 nm), the TPL spectra are acquired as a function of depth (distance between the focal plane and surface). Obviously, photons emitted by radiative recombination will experience reabsorption before being acquired by the detector while propagation from the initial emitting spot (excitation spot) towards the surface (emission collection spot). As shown in Figure 4a and 4b, the PL peak gradually redshifts as the depth increases, due to the increasing number of photon recycling for the detected PL. The TPL spectra at depths of 1 and 30 μm are compared with the one-photon excited PL spectra from the same 2D perovskite with thicknesses of 0.7 and 30 μm, respectively (Figure 4c). The two independent techniques both confirm that the similar PL shift as a function of the distance/thickness between the excitation point and detection emission. The good coincidence of the TPL and PL spectra indicates the similar role of photon transport process in thickness dependent PL and depth dependent TPL. In the TPL measurements, a high quality bulk crystal with a thickness close to one millimetre is investigated. Moreover, the photocarriers are directly generated in the interior region, where defect trapping is expected to be extremely low,[30,57-60] therefore the TPL decay exhibits a minor interference from defect trapping when obtained directly at different depths (≥ 1 μm).

As shown in Figure 4d, the TPL lifetime increases with depth as expected (equation 3), confirming the active role of the photon-recycling process rather than the simple inner filtering (the TPL decay traces are shown in Figure S10, SI). The relationship between lifetime and depth is numerically fitted by the following equation developed by Yamada et al.,[30] in which a carrier diffusion term is absent.

$$\frac{1}{\tau} = \frac{1}{\tau_{max}} + \left(\frac{1}{\tau_{min}} - \frac{1}{\tau_{max}}\right) \exp\left(-\frac{l}{L_0}\right) \qquad (5)$$

l is the depth, τ_{min} corresponds to the TPL lifetime without the photon recycling effect, and τ_{max} corresponds to the limit of the TPL lifetime as $l \rightarrow \infty$. $L_0 = \frac{L_\alpha}{-\ln(\eta_{PR})}$, in which $\eta_{PR} = \eta_{IN}\eta_\alpha$. L_α is the photon propagation length which indicates the average distance travelled by emitted photons propagating through the sample, η_α is the fraction of reabsorbed photons. η_{IN} is the internal luminescence yield, given by

$$\eta_{IN} = \frac{\tau_{max}-\tau_{min}}{\tau_{max}-\eta_\alpha\tau_{min}}. \quad (6)$$

The fitting results give $\tau_{min} = 0.247\ ns$, $\tau_{max} = 0.711\ ns$, and $L_0 = 10.36\ \mu m$. $\eta_{IN} = 0.8$, when assuming $\eta_\alpha = 0.54$ according to the reference.[30] These results from the depth dependent TPL measurements are well consistent with the conclusion that photon recycling is the dominant contributor.

Consequently, the important role of photon recycling for the red-shifted emission is confirmed in 2D perovskites, but it is in the case of the absence of carrier diffusion. The contribution of carrier diffusion is investigated by the transmission-separated detection configuration illustrated in **Figure 5**a. As explained in Figure 5b, the photon propagation lengths are almost identical when separation=0 and 15 μm. Thereby, the additional photon recycling repetition is negligible. It is reasonable no discernible redshift is added in this configuration according to equation (5). However, regarding the PL signal collected from the bottom, the channel for carrier diffusion is switched on/off by the in-plane separation, so that we can solely investigate the contribution of carrier diffusion by ignoring the photon recycling effect. If it is assumed in general 3D perovskites that carrier diffusion is the main pathway for energy transport and produces the redshifted PL with extended lifetime. When the carrier diffusion channel is switched on by the in-plane separation, the PL peak position and the TRPL collected at the bottom should significantly change, because the redshifted peak position and extended lifetime are the two indispensable features for the emission detected after energy transport. However, as shown in Figure 5c and d, no discernible changes can be observed in the

PL peak position and TRPL at different separations (0-15 μm), indicating the carrier diffusion, when it indeed exists in general perovskites, scarcely contributes to the PL collected separated from the excitation spot.

2.3 Depth dependent two-photon photoluminescence of 3D perovskite crystal

We recheck the contribution of photon recycling in general 3D perovskites directly (Figure S11-13, SI). The depth dependent TPL measurements are conducted on a $MAPbBr_3$ single crystal. A similar emission redshift as a function of depth can be observed (**Figure 6**a and 6b). A comparison of the TPL peak positions between 2D perovskite and 3D $MAPbBr_3$ crystal is presented in Figure 6c. The relationships between peak position ($E(l)$) and depth are fitted by exponential decay curves, $E(l) \ = E_{min} + E_0 \exp(-\ l/L_0)$, where $E_{min} + E_0$ and E_{min} are the photon energies of the initial emission without redshift and the emission through a distance l → ∞, respectively (See details in Note S1, SI). $L_0 = 10.02\ \mu m$ is acquired for 2D perovskites, approximately equal to the value acquired from TPL lifetime results. Interestingly, the 3D crystal exhibits a very close L_0 of 11.04 μm. Since the photon recycling related parameters of $MAPbBr_3$ and $(BA)_2PbI_4$ crystals are very similar, such as, bandgap (2.3-2.4 eV), absorption efficiency (10^4-$10^5\ cm^{-1}$),[42] internal PL QY (60-80%),[30,50] refractive index (ca. 1.7-2),[42] and intrinsic stokes-shift (90-100 meV).[42] It is logical to accept the photon recycling terms, η_{PR}, L_α of $MAPbBr_3$ and $(BA)_2PbI_4$ crystals are very close, so they exhibit a similar L_0 value without contribution from carrier diffusion. Even if supposing the contribution of carrier diffusion in the 3D crystal is not negligible, L_0 is expressed as[30] $\sqrt{{L_\alpha}^2 + {L_D}^2 / ln\eta_{PR}}$. However, $L_D \leq 1.055\ \mu m$ (See details in Figure S13, SI) is evidently smaller than L_0 and L_α. Thus, $\sqrt{{L_\alpha}^2 + {L_D}^2} \approx L_\alpha$ suggests L_0 is dominated by L_α and that the long-distance (>L_D) transport of energy in 3D crystals is primarily realized by photon propagation, with prominent role of recycling but insignificant contribution from carrier diffusion. Furthermore, a comparison of the depth-resolved TPL intensity between 2D perovskite and 3D $MAPbBr_3$ crystal is presented in Figure S13, SI. They also exhibit very similar behaviour without apparent indication of carrier diffusion.

2.4 Photoluminescence of cleaved 3D perovskite crystal

Inspired by the 2D perovskite structure, one single 3D bulk $MAPbBr_3$ crystal (thickness ~780 μm) is carefully cleaved into two pieces and then reattached together by an insulating and transparent polymethyl methacrylate (PMMA, ~10 μm) layer. As illustrated in **Figure 7**a, PL and TRPL are measured before and after the cleavage via a transmission mode setup (Figure 1d). In this design, when focusing on energy exchange between the two separated pieces, the carrier diffusion is disabled while photon propagation is still allowable. Again, supposing the PL and the extended lifetime at the rear is purely produced by direct carrier diffusion without photon recycling, as illustrated in the left panel of Figure 7b, the fluorescent photons emitted from the left (L) crystal cannot re-excite the right (R) crystal. Thereby, fluorescence is simply filtered by the R crystal. And the decay becomes faster due to the reduction of diffusion distance from R+L to L after cleavage. As calculated by Beer–Lambert model, the PL band significantly redshifts and almost quenches by the filtering effect (Figure S14). However, as shown in Figure 7c, the PL intensity is a half after cleavage. Besides, both PL peak positions appear at 567 nm without divergence, evidently disagreeing with the carrier diffusion model. The PL lifetime increases after cleavage, which is also contrary to the assumed carrier diffusion model. Whereas, in the photon recycling model (right panel of Figure 7b), after cleavage, the additional reflection and scattering at rough interfaces lead to a longer optical path and more repetitions of photon recycling, as well as an elongated PL lifetime. The rough interface is evidenced in Figure S15. The partially supressed PL intensity is mainly caused by the optical loss at the interfaces. In simple words, if carrier diffusion is a dominant pathway, after cleavage, the PL at the rear should be extremely weak relative to the one before cleavage. However, if energy transport mainly through photon recycling, the cleavage has minor influence on PL from the rear. Apparently, the observation in Figure 7 is the latter case.

3. Discussion

More discussion on carrier distribution, carrier lifetime, and photon energy based on a pure carrier diffusion model are presented in Note S2, Figure S16,17, and Table S2, SI. We find that the main experimental results from both 2D and 3D perovskites exhibit good consistency with the photon recycling model but deviate considerably from the pure carrier diffusion model. Note that high internal PL QY (η_{IN}) is critical for intensive photon recycling.[18,20,30] It is generally accepted that 2D perovskite has a quite high η_{IN} due to strong quantum confinements and large exciton binding energy.[50] The reported external quantum yields are as high as 60%-88%.[61,62] The internal QY is expected to approach unity. Here, the external PL QY (η_{EX}) of our 2D lead halide perovskite crystal is measured to be 23.5%. The η_{IN} is roughly estimated to be about 0.7 according to $\eta_{EX} = \frac{\eta_{IN}/2n_r^2}{\frac{\eta_{IN}}{2n_r^2}+(1-\eta_{IN})+L/4\alpha_0 d_0}$, which is close to the value acquired from lifetime by equation (6). α_0 and d_0 are average absorption coefficient and absorber thickness, respectively. $L = 1 - reflectivity$ is the loss factor. n_r (ca.1.7) is the average refractive index.[63] Yamada et al have verified $\eta_{IN} = 0.85$ is sufficient for intensive photon recycling.[30] As demonstrated by Abebe et al,[20] when η_{IN} is higher than 0.3, efficient photon recycling is expected, even adequately enhancing the open-circuit voltage. Absorption coefficient, Stokes-shift and refractive index are also vital parameters determining the degree of photon recycling. The evident waveguiding effect (Figure S6), high refractive index (Figure S7) and entire overlaps between emission and absorption spectra (Figure S18) suggest photon recycling is much easier in perovskites compared to other conventional semiconductors.

Obviously, the carrier diffusion and photon recycling cannot be strictly separated in the 3D perovskites. When emission is reabsorbed in the interior, carriers are re-generated, resulting in a redistribution of carriers locally. Nevertheless, based on the solid evidence presented and the discussion, we emphasize in this work that the observation of PL separated from the excitation spot is mainly realized by photon transport instead of pure carrier diffusion. It should be noted the clarification of this issue is very crucial for the correct evaluation of carrier dynamics and thus the performance of perovskite based photovoltaic and photonic devices. As demonstrated, ignoring photon recycling may lead to a serious underestimation of the open-circuit voltage (measured value> theoretical value).[20,64] Moreover, one of the most important factors proposed for the high efficiency of perovskite solar cells is their long carrier diffusion length. An insufficient understanding of the dominant role of photon recycling will result in an overestimation of the intrinsic carrier diffusion length (measured value> the intrinsic value). For the same $MAPbBr_3$ crystal investigated in this work, if the PL lifetime is measured by reflection mode, carrier diffusion length (L_D) is no longer than 1.055 μm, whereas $L_D = 2.857$ μm if carrier lifetime is measured by transmission mode ($\tau_{eff} = 2.72\, ns$) due to photon recycling. Importantly, even for common reflection geometry, photon recycling is also involved.[20,39] The "long" carrier diffusion lengths of perovskites include a significant contribution from photon recycling. In other words, the photon recycling should be carefully excluded in all the measurements of intrinsic carrier lifetime/diffusion length by an optical method.

Our finding also will benefit the device designs and improvements. For solar cells, carrier diffusion and photon recycling imply different impacts on open-circuit voltage. Previous calculations revealed photon recycling will induce an additional open-circuit voltage value up to 240 mV.[20] Whereas, high diffusion coefficients may reduce V_{OC} in the presence of nonradiative surface recombination.[65] However, regarding LEDs, highly efficient photon recycling generally implies a low out-coupling probability, which is a bottleneck for light output. Currently, the lack of awareness on the dominant role of photon recycling, resulting in a neglect of photon out-coupling effect, thus hinders the developments of LEDs. For example, although much effort has been made, the state of art external quantum efficiencies (EQEs) of 2D perovskites based LEDs are only around 10%,[10,62,66] which are remarkably lower than EQE of CdSe–CdS core–shell quantum dots (20.5%).[67] Until very recently, the EQE of perovskites based LED is largely improved to 20.7% via enhancing the extract of the trapped light.[68] In other optoelectronic devices, such as luminescent solar concentrators, photon recycling is also a pivotal factor should be considered.[69] To make our conclusions convincing while keep the paper readable, more discussion are presented in Note S3, SI.

4. Conclusion

In summary, a common controversy in the photophysics of perovskites has been addressed in this work. To date, in order to explain the special properties of the perovskites, carrier diffusion or photon recycling, or both are adopted to describe the dynamics of carriers, leading to a considerable confusion. In this work, firstly, the Ruddlesden−Popper type perovskite, where inter-plane carrier diffusion is negligible due to the intercalation with organic spacers, is investigated. Nevertheless, a remarkable PL redshift still occurs in the vertical direction with increasing thickness, which is generally explained by the photon transport. An ordinary 3D perovskite has been comparatively studied by the depth-resolved TPL spectra. Compared to carrier diffusion, photon recycling is a dominant photophysical process that accounts for the experimental observations and long-distance energy transport in both 2D and 3D halide perovskites. The clarification of this issue will have significant impact on the mechanistic understanding, and future development of photovoltaics, LEDs and diverse other optoelectronic devices based on perovskites.

5. Experimental Section

Synthesis of 2D BA_2PbI_4 crystals

The synthesis of BA_2PbI_4 single crystals is based on the method by Stoumpos et al. with some modifications.[45] Lead acetate ($Pb(COO)_2$) powder (1.6 g) was dissolved in 5 mL of 57%

w/w aqueous hydroiodic acid (HI) solution at room temperature under constant magnetic stirring, which formed a bright yellow solution. Meanwhile, in another bottle, n-$CH_3(CH_2)_3NH_2$ (0.9 mL) was slowly neutralized with 5 mL of HI 57% w/w in an ice bath. Then, the n-$CH_3(CH_2)_3NH_3I$ solution was dropwise added to the lead solution under 100 ^oC and stirring, which initially produced a black precipitate, and subsequently dissolved under heating the combined solution to boiling. The stirring was then stopped, and the solution was left to cool to room temperature during which time orange plate shaped crystals can be obtained. The precipitation was deemed to be complete after about 2 hours. The crystals were isolated by filtration and thoroughly dried under reduced pressure. The 2D perovskite platelets were obtained by cleaving the bulk crystals using the well-known scotch-tape method under the protection of nitrogen. To avoid the structural degradation, the samples were freshly prepared for all the measurements. A commercial type NT-MDT AFM was used to determine the thickness of the acquired platelets.

Synthesis of 3D $CH_3NH_3PbBr_3$ crystals

The solution of the bromide salts (1 M) in dimethylformamide was prepared firstly. Then 3 vol% of formic acid was added to the solution followed by a filtration with 0.45 μm filter. A 5 ml portion of the solution was then incubated in a closed cap vial at 55 °C to produce some seed crystals (~500 μm scale). In another vial, a cleaned Si wafer was placed at the bottom of the vial with fresh salt solutions. Finally, the as prepared seed crystal of $CH_3NH_3PbBr_3$ was put on the substrate with further incubation at 55 °C. The seed crystal grew on the Si substrate and we collected it when it had the desired size.

Structural characterization

TEM characterization was performed with a JEOL 2010UHR operated at 200 kV. Powder XRD pattern of the crystal was recorded on Bruker D8 diffractometer at a scanning rate of 1° min^{-1}, using Cu Kα radiation (λ=1.5406 Å). The optical microscopic images were captured by an inverted metallurgical microscope equipped with a CCD camera (Nikon Eclipse MA100).

Optical spectroscopy

Absorption spectra recorded on a Perkin Elmer Lambda1050 spectrophotometer coupled with an integrating sphere. Steady-state and time-resolved photoluminescence measurements were performed with a time-correlated single photon counting system (PicoHarp 300, PicoQuant GmbH). A 405 nm laser diode (pulse duration 40 ps) was used as the excitation source (0.1 $\mu J/cm^2$). For the excitation depth dependent TPL measurements, a 960 nm femtosecond laser (pulse width of 100 fs, Mai Tai) was used for excitation. The focal position of a microscope (a modified Leica TCS SP5 microscope) was adjusted to probe TPL at various depths. The depth resolution in the z-direction is approximately 500 nm. A 100× objective lens was used to focus the excitation light and collect the fluorescence through a pinhole of 100 μm diameter.

Supporting Information

Supporting Information is available from the Wiley Online Library or from the author.

Acknowledgements

X.W. and B.J. acknowledges the support from the Australian Research Council (DP150104327, DP150102972, and DP160102955). Z.G. acknowledges support from the National Natural Science Foundation of China (No. 11604155). K.P.G. acknowledges support from the ARC Centre of Excellence in Exciton Science (CE170100026). H.Z. thanks the support from MOE under AcRF Tier 2 (ARC 19/15, No. MOE2014-T2-2-093; MOE2015-T2-2-057; MOE2016-T2-2-103; MOE2017-T2-1-162) and AcRF Tier 1 (2016-T1-001-147; 2016-T1-002-051; 2017-T1-001-150; 2017-T1-002-119), and NTU under Start-Up Grant (M4081296.070.500000) in Singapore.

Received: ((will be filled in by the editorial staff))
Revised: ((will be filled in by the editorial staff))
Published online: ((will be filled in by the editorial staff))

References

[1] M. M. Lee. J. Teuscher, T. Miyasaka, T. N. Murakami, H. J. Snaith, *Science* **2012**, *338*, 643.

[2] D. P. McMeekin, G. Sadoughi, W. Rehman, G. E. Eperon, M. Saliba, M. T. Hörantner, A. Haghighirad, N. Sakai, L. Korte, B. Rech, M. B. Johnston, L. M. Herz, H. J. Snaith. *Science* **2016**. *351*, 151.

[3] J. H. Heo, S. H. Im, J. H. Noh, T. N. Mandal, C.-S. Lim, J. A Chang, Y. H. Lee, H.-j. Kim, A. Sarkar, Md. K. Nazeeruddin, M. Grätzel , S. Il Seok, *Nat. Photon.* **2013**, *7*, 486.

[4] M. A. Green, A. Ho-Baillie, H. J. Snaith, *Nat. Photon.* **2014**, *8*, 506.

[5] H. J. Snaith, *Nat. Mater.* **2018**, *17*, 372.

[6] C. Eames, J. M. Frost, P. R. F. Barnes, B. C. O'Regan, A. Walsh, M. S. Islam, *Nat. Commun.* **2015**, *6*, 7497.

[7] J. Xiao, J. Shi, H. Liu, Y. Xu, S. Lv, Y. Luo, D. Li, Q. Meng, Y. Li, *Adv. Energy Mater.* **2015**, *5*, 1401943.

[8] Z.-K. Tan, R. S. Moghaddam, M. L. Lai, P. Docampo, R. Higler, F. Deschler, M. Price, A. Sadhanala, L. M. Pazos, D. Credgington, F. Hanusch, T. Bein, H. J. Snaith, R. H. Friend, *Nat. Nanotechnol.* **2014**, *9*, 687.

[9] H. Cho, S.-H. Jeong, M.-H. Park, Y.-H. Kim, C. Wolf, C.-L. Lee, J. H. Heo, A. Sadhanala, N. Myoung, S. Yoo, S. H. Im, R. H. Friend, T.-W. Lee, *Science* **2015**, *350*, 1222.

[10] M. Yuan, L. N. Quan, R. Comin, G. Walters, R. Sabatini, O. Voznyy, S. Hoogland, Y. Zhao, E. M. Beauregard, P. Kanjanaboos, Z. Lu, D. H. Kim, E. H. Sargent, *Nat. Nanotechnol.* **2016**, *11*, 872.

[11] X. Hu, X. Zhang, L. Liang, J. Bao, S. Li, W. Yang , Y. Xie, *Adv. Funct. Mater.* **2014**, *24*, 7373.

[12] S. F. Leung, K.T. Ho, P. K. Kung, V. K. S. Hsiao, H. N. Alshareef, Z. L. Wang, J. H. He, *Adv. Mater.* **2018**, *30*, 1704611.

[13] J. Lu, X. Sheng, G. Tong, Z. Yu, X. Sun, L. Yu, X. Xu, J. Wang, J. Xu, Y. Shi, K. Chen, *Adv. Mater.* **2017**, *29*, 1700400.

[14] G. Xing, N. Mathews, S. S. Lim, N. Yantara, X. Liu, D. Sabba, M. Grätzel, S. Mhaisalkar, T. C. Sum, *Nat. Mater.* **2014**, *13*, 476.

[15] Jia, Y. R. A. Kerner, A. J. Grede, A. N. Brigeman, B. P. Rand, N. C. Giebink, *Nano Lett.* **2016**, *16*, 4624.

[16] B. Tang, H. Dong, L. Sun, W. Zheng, Q. Wang, F. Sun, X. Jiang, A. Pan, L. Zhang, *ACS Nano* **2017**, *11*, 10681.

[17] Y. Jia, R. A. Kerner, A. J. Grede, B. P. Rand, N. C. Giebink, *Nat. Photon.* **2017**, *11*, 784.

[18] J. M. Richter, M. Abdi-Jalebi, A. Sadhanala, M. Tabachnyk, J. P.H. Rivett, L. M. Pazos-Outón, K. C. Gödel, M. Price, F. Deschler, R. H. Friend, *Nat. Commun.* **2016**, *7*, 13941.

[19] L. M. Pazos-Outón, M. Szumilo, R. Lamboll, J. M. Richter, M. Crespo-Quesada, M. Abdi-Jalebi, H. J. Beeson, M. Vrućinić, M. Alsari, H. J. Snaith, B. Ehrler, R. H. Friend, F. Deschler, *Science* **2016**, *351*, 1430.

[20] Abebe, M. G. A. Abass, G. Gomard, L. Zschiedrich, U. Lemmer, B. S. Richards, C. Rockstuhl, U. W. Paetzold, *Phys. Rev. B*, **2018**, *98*, 075141.

[21] T. Kirchartz, F. Staub, U. Rau, *ACS Energy Lett.* **2016**, *1*, 731.

[22] Xing, G. N. Mathews, S. Sun, S. S. Lim, Y. M. Lam, M. Grätzel, S. Mhaisalkar, T. C. Sum, *Science* **2013**, *342*, 344.

[23] S. D. Stranks, G. E. Eperon, G. Grancini, C. Menelaou, M. J. P. Alcocer, T. Leijtens, L. M. Herz, A. Petrozza, H. J. Snaith, *Science* **2013**, *342*, 341.

[24] Z. Xiao, Q. Dong, B. Cheng, Y. Shao, J. Huang, *Adv. Mater.* **2014**, *26*, 6503.

[25] Q. Dong, Y. Fang, Y. Shao, P. Mulligan, J. Qiu, L. Cao, J. Huang, *Science* **2015**, *347*, 967.

[26] W. S. Yang, B.-W. Park, E. H. Jung, N. J. Jeon, Y. C. Kim, D. U. Lee, S. S. Shin, J. Seo, E. K. Kim, J. H. Noh , S. I. Seok, *Science* **2017**, *356*, 1376.

[27] G. Hodes, P. V. Kamat, *J. Phys. Chem. Lett.* **2015**, *6*, 4090.

[28] S. D. Wolf, J. Holovsky, S.-J. Moon, P. Löper, B. Niesen, M. Ledinsky, F.-J. Haug, J.-H. Yum, C. Ballif, *J. Phys. Chem. Lett.* **2014**, *5*, 1035.

[29] E. T. Hoke, D. J. Slotcavage, E. R. Dohner, A. R. Bowring, H. I. Karunadasa, M. D. McGehee, *Chem. Sci.* **2015**, *6*, 613.

[30] T. Yamada, Y. Yamada, Y. Nakaike, A. Wakamiya, Y. Kanemitsu, *Phys. Rev. Appl.* **2017**, *7*, 014001.

[31] H. Diab, C. Arnold, F. Lédée, G. Trippé-Allard, G. Delport, C. Vilar, F. Bretenaker, J. Barjon, J.-S. Lauret, E. Deleporte, D. Garrot. *J. Phys. Chem. Lett.* **2017**, *8*, 2977.

[32] Y. Yamada, T. Yamada, L. Q. Phuong, N. Maruyama, H. Nishimura, A. Wakamiya, Y. Murata , Y. Kanemitsu, *J. Am. Chem. Soc.* **2015**, *137*, 10456.

[33] T. W. Crothers, R. L. Milot, J. B. Patel, E. S. Parrott, J. Schlipf, P. Müller-Buschbaum, M. B. Johnston, L. M. Herz, *Nano Lett.* **2017**, *17*, 5782.

[34] T. Yamada, Y. Yamada, H. Nishimura, Y. Nakaike, A. Wakamiya, Y. Murata , Y. Kanemitsu, *Adv. Electron. Mater.* **2016**, *2*, 1500290.

[35] Z. X. Gan, W. J. Chen, L. Yuan, G. Y. Cao, C. H. Zhou, S. J. Huang, X. M. Wen and B. H. Jia, *Appl. Phys. Lett.* **2019**, *114*, 011906.

[36] J. Shi, H. Zhang, Y. Li, J. J. Jasieniak, Y. Li, H.Wu, Y. Luo, D. Li, and Q. Meng, *Energy Environ. Sci.* **2018**, *11*, 1460.

[37] M. R. Khan, X. Wang, R. Asadpour, M. Lundstrom, M. A. Alam, arXiv:1612.06731

[38] M. Ansari-Rad, J. Bisquert, *Phys. Rev. Appl.* **2018**, *10*, 034062.

[39] Y. Fang, H. Wei, Q. Dong, J. Huang, *Nat. Commun.* **2017**, *8*, 14417.

[40] Y. Fang, Q. Dong, Y. Shao, Y. Yuan , J. Huang, *Nat. Photon.* **2015**, *9*, 679.

[41] Y. Bi, E. M. Hutter, Y. Fang, Q. Dong, J. Huang , T. J. Savenije, *J. Phys. Chem. Lett.* **2016**, *7*, 923.

[42] B. Wenger, P. K. Nayak, X. Wen, S. V. Kesava, N. K. Noelm, H. J. Snaith, *Nat. Commun.* **2017**, *8*, 590.

[43] W. Tian, C. Zhao, J. Leng, R. Cui, S. Jin, *J. Am. Chem. Soc.* **2015**, *137*, 12458.

[44] D. Lan, M. A. Green, *J. Appl. Phys.* **2014**, *116*, 174511.

[45] C. C. Stoumpos, D. H. Cao, D. J. Clark, J. Young, J. M. Rondinelli, J. I. Jang, J. T. Hupp, M. G. Kanatzidis, *Chem. Mater.* **2016**, *28*, 2852.

[46] L. Dou, A. B. Wong, Y. Yu, M. Lai, N. Kornienko, S. W. Eaton, A. Fu, C. G. Bischak, J. Ma, T. Ding, N. S. Ginsberg, L.-W. Wang, A. P. Alivisatos, P. Yang, *Science* **2015**, *349*, 1518.

[47] J. C. Blancon, H. Tsai, W. Nie, C. C. Stoumpos, L. Pedesseau, C. Katan, M. Kepenekian, C. M. M. Soe, K. Appavoo, M. Y. Sfeir, S. Tretiak, P. M. Ajayan, M. G. Kanatzidis, J. Even, J. J. Crochet, A. D. Mohite, *Science* **2017**, *355*, 1288.

[48] S. Yang, W. Niu, A. L. Wang, Z. Fan, B. Chen, C. Tan, Q. Lu , H. Zhang, *Angew. Chem. Int. Ed.* **2017**, *56*, 4252.

[49] I. Abdelwahab, G. Grinblat, K. Leng, Y. Li, X. Chi, A. Rusydi, S. A. Maier, K. P. Loh, *ACS Nano* **2018**, *12*, 644.

[50] G. Xing, B. Wu, X. Wu, M. Li, B. Du, Q. Wei, J. Guo, E. K. L. Yeow, T. C. Sum, W. Huang, *Nat. Commun.* **2017**, *8*, 14558.

[51] X. Wen, Y. Feng, S. Huang, F. Huang, Y.-B. Cheng, M. Green, A. Ho-Baillie, *J. Mater. Chem. C* **2016**, *4*, 793.

[52] S. D. Stranks, V. M. Burlakov, T. Leijtens, J. M. Ball, A. Goriely, H. J. Snaith, *Phys. Rev. Appl.* **2014**, *2*, 034007.

[53] D. Miller, E. Yablonovitch, S. R. Kurtz, *IEEE J. Photovoltaics* **2012**, *2*, 303.

[54] L. Zhu, T. Mochizuki, M. Yoshita, S. Chen, C. Kim, H. Akiyama , Y. Kanemitsu, *Opt. Express* **2016**, *24*, A740.

[55] J. S. Yun, A. Ho-Baillie, S. Huang, S. H. Woo, Y. Heo, J. Seidel, F. Huang, Y.-B. Cheng, M. A. Green, *J. Phys. Chem. Lett.* **2015**, *6*, 875.

[56] K. J. Karki, M. Abdellah, W. Zhang, T. Pullerits, *APL Photonics* **2016**, *1*, 046103.

[57] Y. Yang, Y. Yan, M. Yang, S. Choi, K. Zhu, J. M. Luther, M. C. Beard, *Nat. Commun.* **2015**, *6*, 7961.

[58] X. Wu, M. T. Trinh, D. Niesner, H. Zhu, Z. Norman, J. S. Owen, O. Yaffe, B. J. Kudisch , X.-Y. Zhu, *J. Am. Chem. Soc.* **2015**, *137*, 2089.

[59] W. Chen, X. Wen, M. Latzel, M. Heilmann, J. Yang, X. Dai, S. Huang, S. Shrestha, R. Patterson, S. Christiansen , G. Conibeer, *ACS Appl. Mater. Interfaces* **2016**, *8*, 31887.

[60] X. Wen, P. Xu, P. B. Lukins , N. Ohno, *Appl. Phys. Lett.* **2003**, *83*, 425.

[61] K. Zheng, Y. Chen, Y. Sun, J. Chen, P. Chábera, R. Schaller, M. J. Al-Marri, S. E. Canton de, Z. Liang, T. Pullerits, *J. Mater. Chem. A* **2018**, *6*, 6244.

[62] J. Xing, Y. Zhao, M. Askerka, L. N. Quan, X. Gong, W. Zhao, J. Zhao, H. Tan, G. Long, L. Gao, Z. Yang, O. Voznyy, J. Tang, Z.-H. Lu, Q. Xiong , E. H. Sargent, *Nat. Commun.* **2018**, *9*, 3541.

[63] I. L. Braly, D. W. deQuilettes, L. M. Pazos-Outón, S. Burke, M. E. Ziffer, D. S. Ginger, H. W. Hillhouse, *Nat. Photon.* **2018**, *12*, 355.

[64] A. W. Walker, O. Hohn, D. N. Micha, B. Blasi, A. W. Bett, F. Dimroth, *IEEE J. Photovoltaics* **2015**, *5*, 1636.

[65] S. D. Stranks, *ACS Energy Lett.* **2017**, *2*, 1515.

[66] N. Wang, L. Cheng, R. Ge, S. Zhang, Y. Miao, W. Zou, C. Yi, Y. Sun, Y. Cao, R. Yang, Y. Wei, Q. Guo, Y. Ke, M. Yu, Y. Jin, Y. Liu, Q. Ding, D. Di, L. Yang, G. Xing, H. Tian, C. Jin, F. Gao, R. H. Friend, J. Wang, W. Huang, *Nat. Photon.* **2016**, *10*, 699.

[67] X. Dai, Z. Zhang, Y. Jin, Y. Niu, H. Cao, X. Liang, L. Chen, J. Wang, X. Peng, *Nature* **2014**, *515*, 96.

[68] Y. Cao, N. Wang, H. Tian, J. Guo, Y. Wei, H. Chen, Y. Miao, W. Zou, K. Pan, Y. He, H. Cao, Y. Ke, M. Xu, Y. Wang, M. Yang, K. Du, Z. Fu, D. Kong, D. Dai, Y. Jin, G. Li, H. Li, Q. Peng, J. Wang, W. Huang, *Nature* **2018**, *562*, 249.

[69] F. Meinardi, Q. A. Akkerman, F. Bruni, S. Park, M. Mauri, Z. Dang, L. Manna, S. Brovelli, *ACS Energy Lett.* **2017**, *2*, 2368.

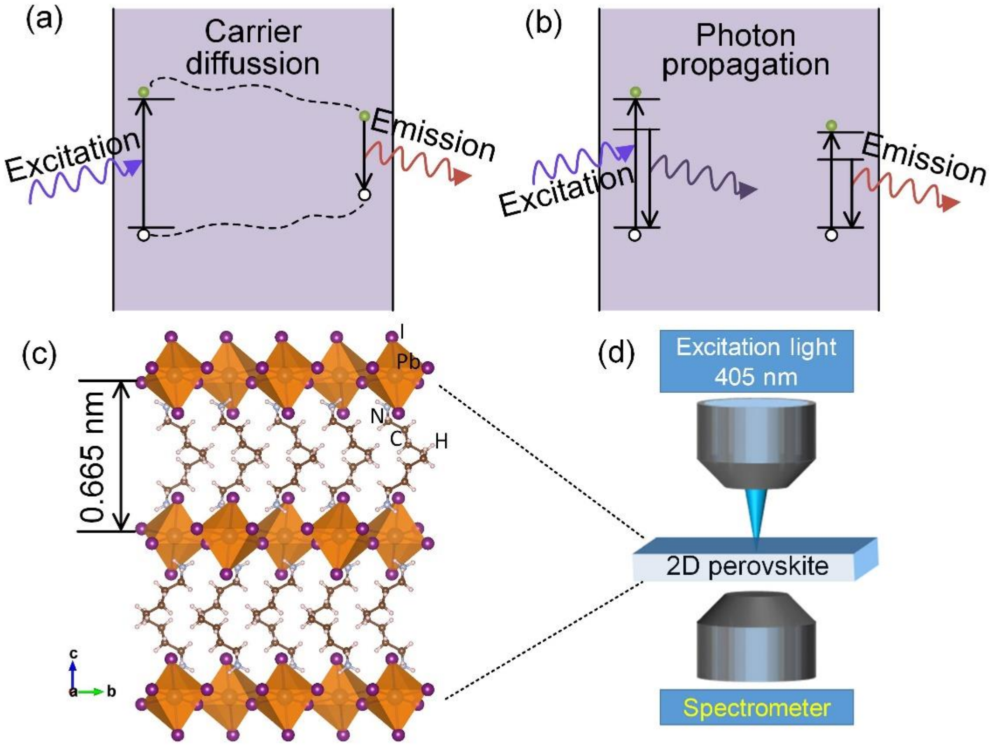

Figure 1. Scheme of the carrier diffusion, photon recycling and the measurement method. (a,b) Schematic illustrations of carrier diffusion (a) and photon recycling (b). (c) Crystal structure of the 2D $(BA)_2PbI_4$ lead iodide perovskite. (d) Representation of the instrument geometry for PL/TRPL measurements via a transmission mode.

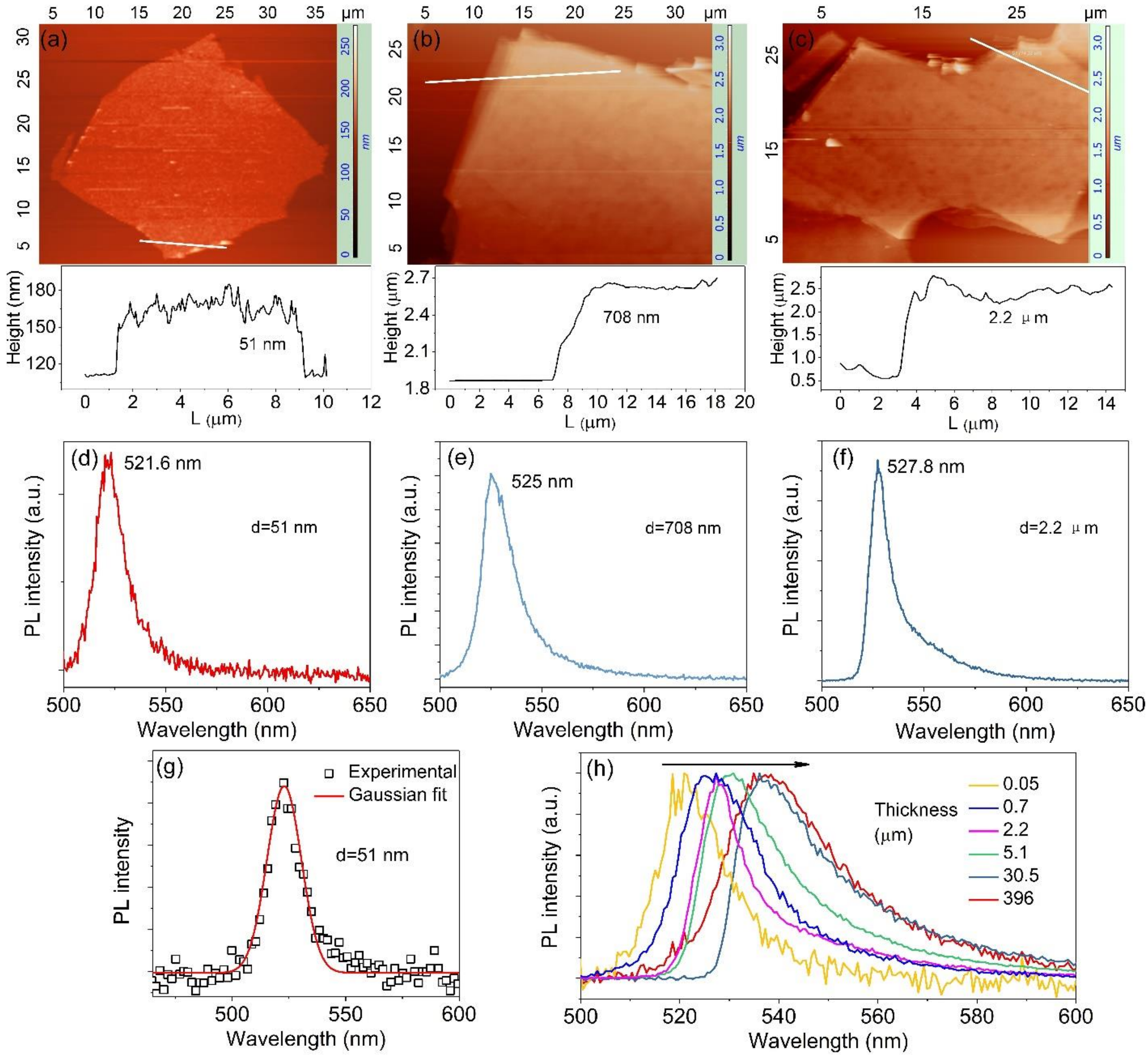

Figure 2. (a-c) AFM images of the 2D perovskite platelets with different thicknesses. The corresponding height profiles are shown in the following panels. (d-f) PL spectra of the 2D perovskite platelets with thicknesses of 51 nm (d), 708 nm (e), and 2.2 µm (f). (g) Gaussian fit of the symmetric PL obtained from the 51 nm-thick perovskite platelet. (h) PL spectra of the 2D perovskites with different thicknesses.

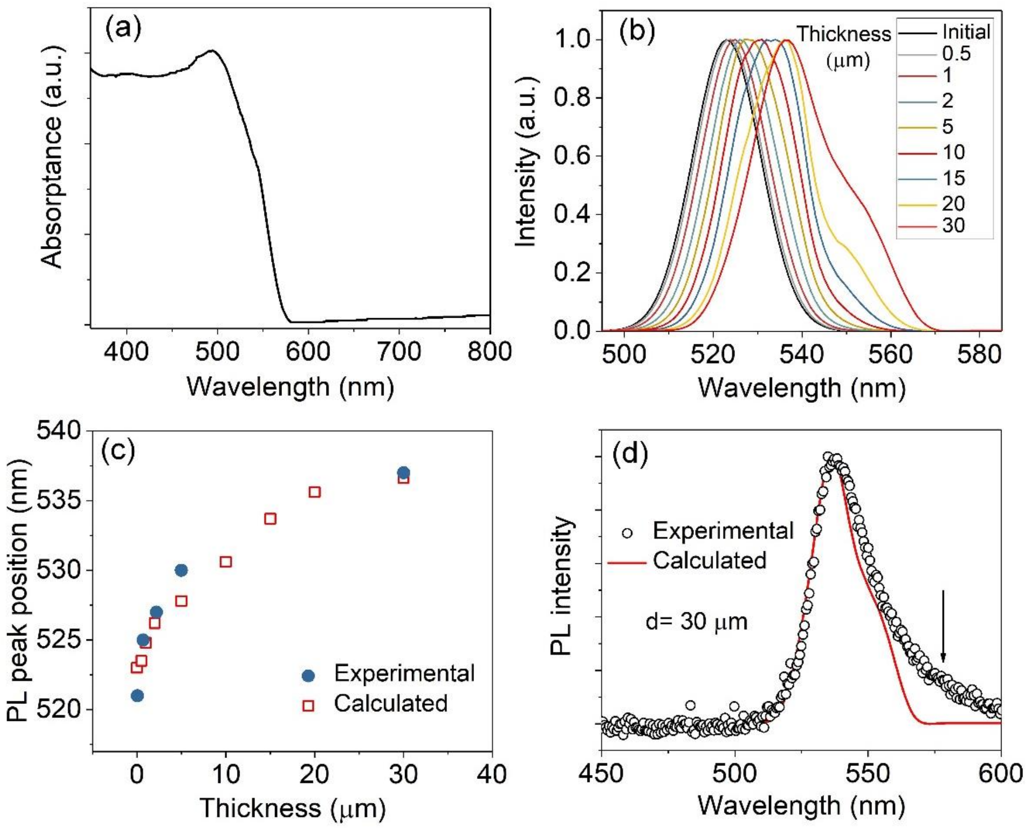

Figure 3. (a) Absorption spectrum of a 2D perovskite crystal. (b) Calculated PL spectra at different thicknesses based on the Beer-Lambert prediction. (c) Relationship between PL peak position and thickness, the open squares and solid circles represent calculated and experimental results, respectively. (d) Comparison of the normalized PL spectra from measurement (black circles) and calculation (red line) when d=30 μm.

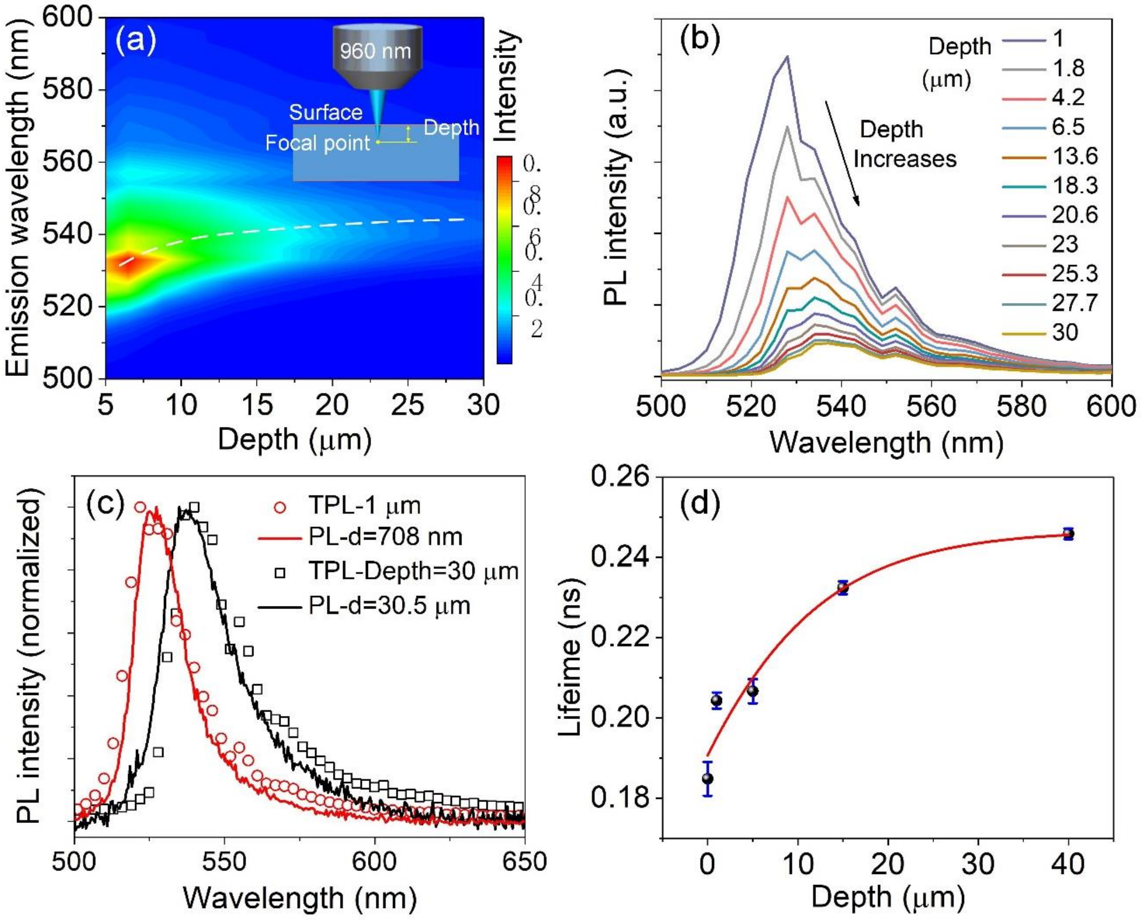

Figure 4. Depth resolved TPL spectra of 2D perovskites. (a) Emission contour map at different depths. Inset: Graphical representation of the setup for depth-resolved TPL measurements. (b) TPL spectra acquired from a bulk sample at different depths. (c) Comparison of the PL spectra from two thicknesses (lines) and TPL spectra from two depths (scattered points). (d) Lifetimes with error bars at different excitation depths. The red line is the fitted curve based on equation (5).

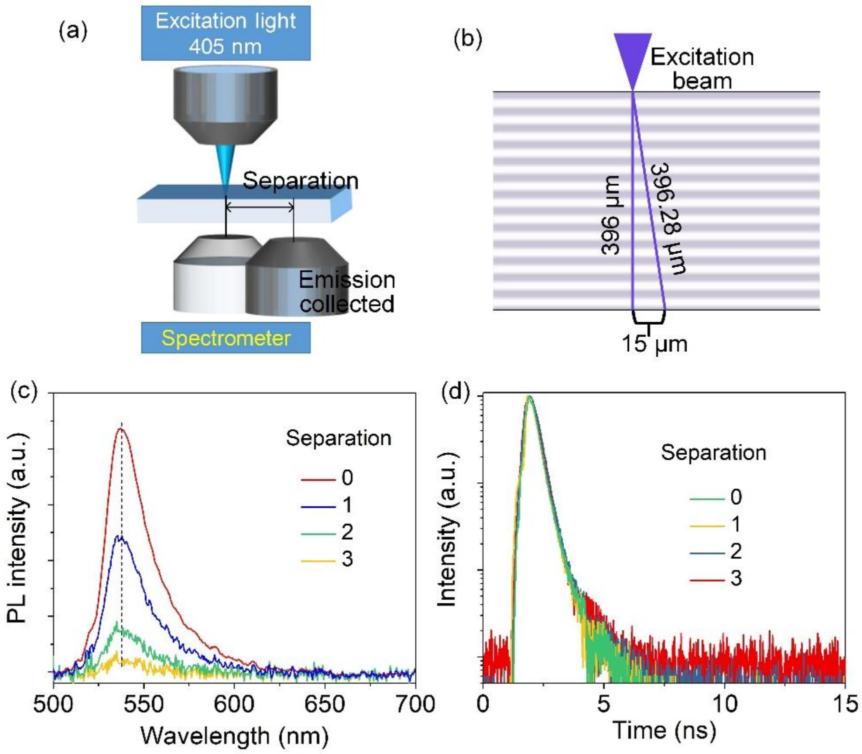

Figure 5. (a) The scheme illustrates that emission objective was slightly moved in horizontal direction to collect the PL spectra. (b) In this configuration, the photon propagation lengths are almost unchanged since the thickness of the crystal (396 µm) is much larger than the separation. While if separation is not 0, the channel of carrier diffusion is switched on. (c) PL spectra of a bulk 2D crystal acquired at different separations (Separation step 0-3 represents 0-15 µm). (d) TRPL spectra acquired at different separations (0-15 µm).

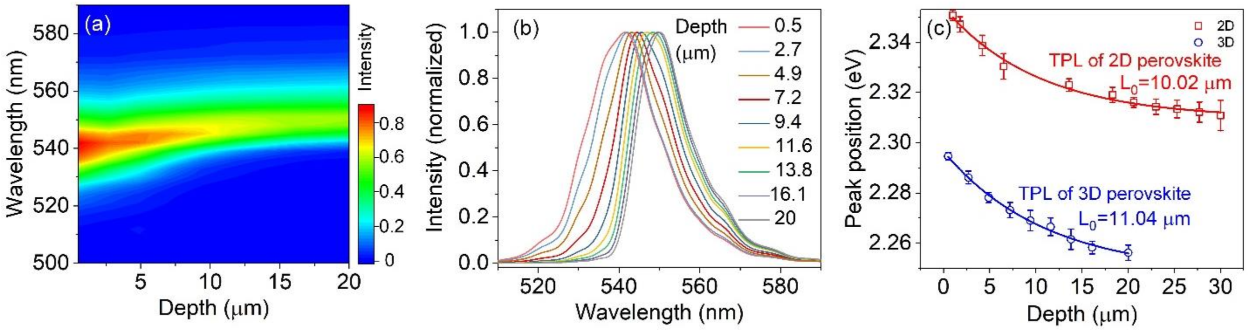

Figure 6. Depth resolved TPL spectra of a 3D $MAPbBr_3$ single crystal. (a) Emission contour map at different depths. (b) Normalized TPL spectra acquired from a $MAPbBr_3$ crystal at different depths. (c) A comparison of the depth resolved TPL peak positions of 2D perovskites (squares) and 3D $MAPbBr_3$ crystal (circles).

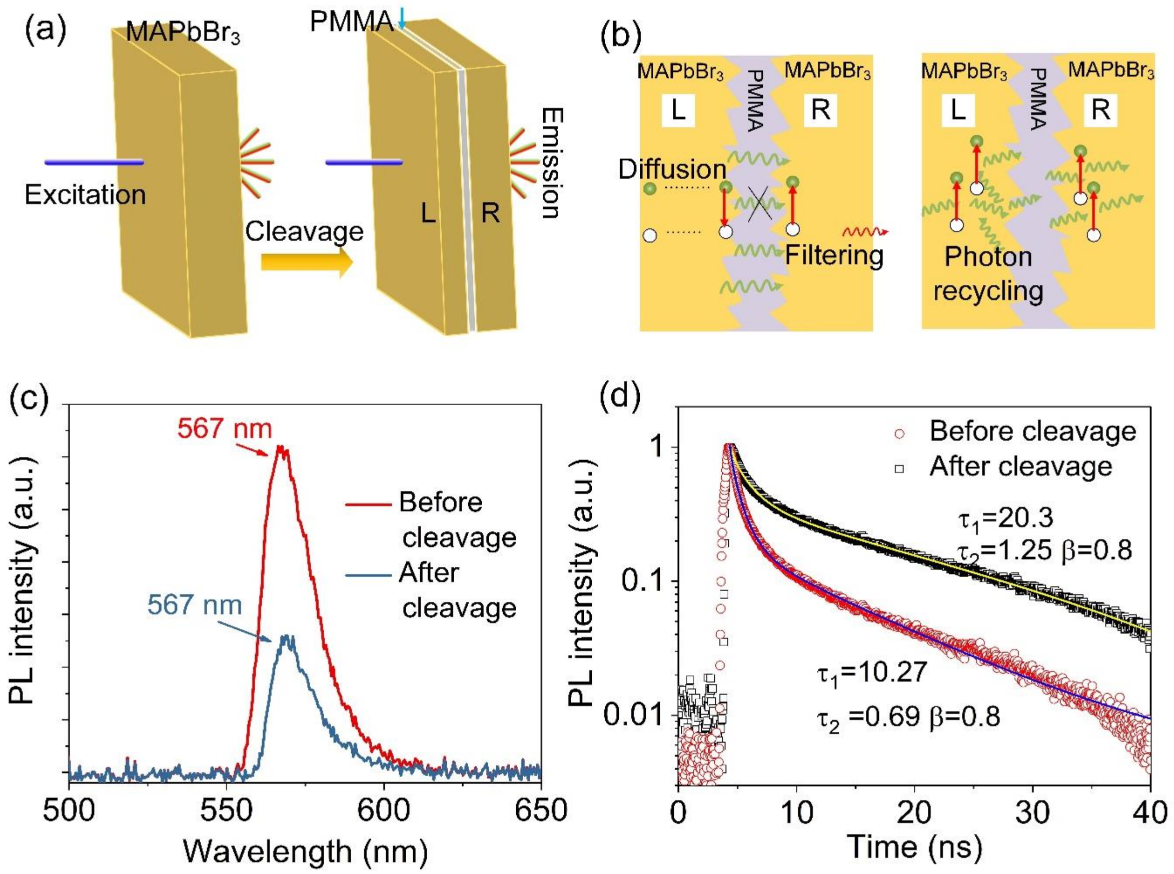

Figure 7. PL and TRPL of a cleaved 3D $MAPbBr_3$ crystal. (a) Scheme illustrating the cleavage of 3D $MAPbBr_3$ crystal. (b) A comparison of pure carrier diffusion and photon recycling models at the PMMA interfaces, the two pieces of crystals are designated as L and R for ease of discussion. (c,d) PL (c) and TRPL (d) of a 3D $MAPbBr_3$ before and after cleavage. The solid line represents fitting by a stretched-exponential function.

Photon recycling and carrier diffusion are the two plausible processes that primarily affect the carrier dynamics in halide perovskites, and therefore the evaluation of the performance of their photovoltaic and photonic devices. However, it is still challenging to isolate their individual contributions because both processes result in a similar emission redshift. Herein, we confirm that photon recycling is the dominant effect responsible for the observed redshifted emission.

Keyword Energy transport

Zhixing Gan, Xiaoming Wen,* Weijian Chen, Chunhua Zhou, Shuang Yang, Guiyuan Cao, Kenneth P. Ghiggino, Hua Zhang and Baohua Jia*

The Dominant Energy Transport Pathway in Halide Perovskites: Photon Recycling or Carrier Diffusion?

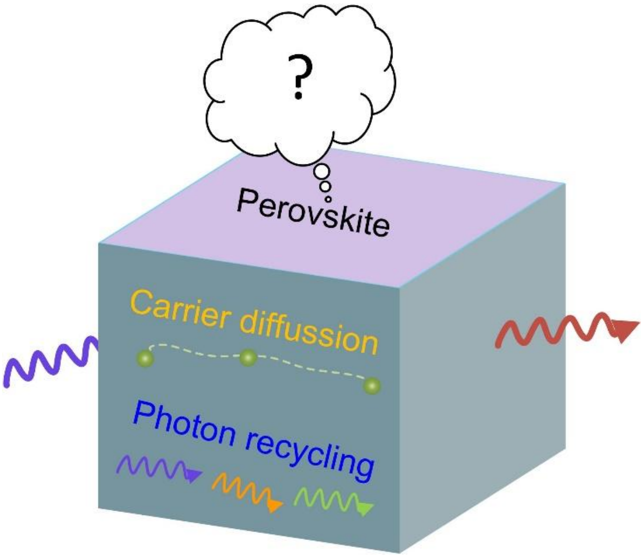

ToC figure

Supporting Information

The Dominant Energy Transport Pathway in Halide Perovskites: Photon Recycling or Carrier Diffusion?

Zhixing Gan, Xiaoming Wen, Weijian Chen, Chunhua Zhou, Shuang Yang, Guiyuan Cao, Kenneth P. Ghiggino, Hua Zhang and Baohua Jia**

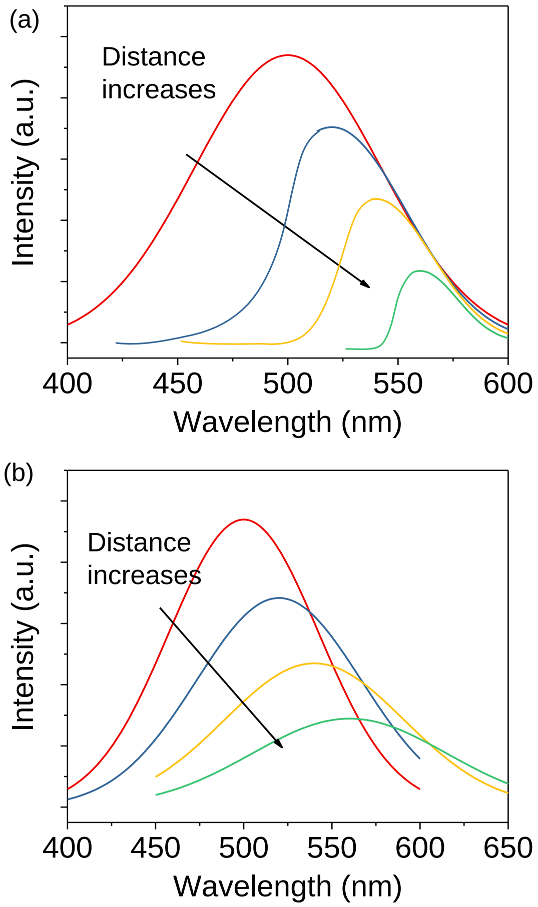

Figure S1. Schematic drawing of PL spectra redshift caused by photon reabsorption (a) and photon recycling (b).

For the photon reabsorption effect, the PL excited on the surface of the single crystal is absorbed during its transmission through the crystal. When the quantum yield is very low, the re-emission generated by reabsorption can be ignored. In this case, the PL at higher energy is sharply reduced while longer wavelength emission is not affected as transmission distance increases (Figure S1a). Meanwhile, the FWHM evidently narrows and PL lifetime is not affected. The photon recycling effect contains both reabsorption and re-emission. Thus, not only high energy PL is filtered, but also more low-energy photons are re-generated (Figure S1b) and the PL lifetime increases according to equation (3). The photon-recycling induced emission redshift contains two contributions, one follows the probability convoluted with the thermal activation energy available in the film and the other one is the spectral filtering. The former one is weak as commented. Therefore, the PL redshift is mainly caused by spectral filtering. Thus, the PL spectra with photon-recycling and photon reabsorption (pure spectral filtering) are quite similar.

In our experiment, the collected emission includes both the filtered photons (photon reabsorption) and recycled photons (photon recycling). The quantification of photon reabsorption and recycling has been investigated by Fang et al previously,[1] which is not the main target of this paper. However, firstly, the broadened PL spectra shown in Figure 2h, comparison of the experimental/calculated PL spectra shown in Figure 3d, and extended PL lifetime shown in Figure 4d exhibit photon recycling features. Secondly, our following results throughout the paper confirm the collected emission contains an insignificant contribution of direct carrier diffusion. In particular, the carrier diffusion is largely excluded in the perpendicular direction of 2D perovskites. Therefore, photon recycling plays a much dominant role than carrier diffusion for energy transport. As highlighted in the main text, photon recycling will lead to an extended PL lifetime (not the actual carrier lifetime), thus, an overestimation of intrinsic carrier diffusion length. Thus, our results emphasize the photon recycling rather than photon reabsorption.

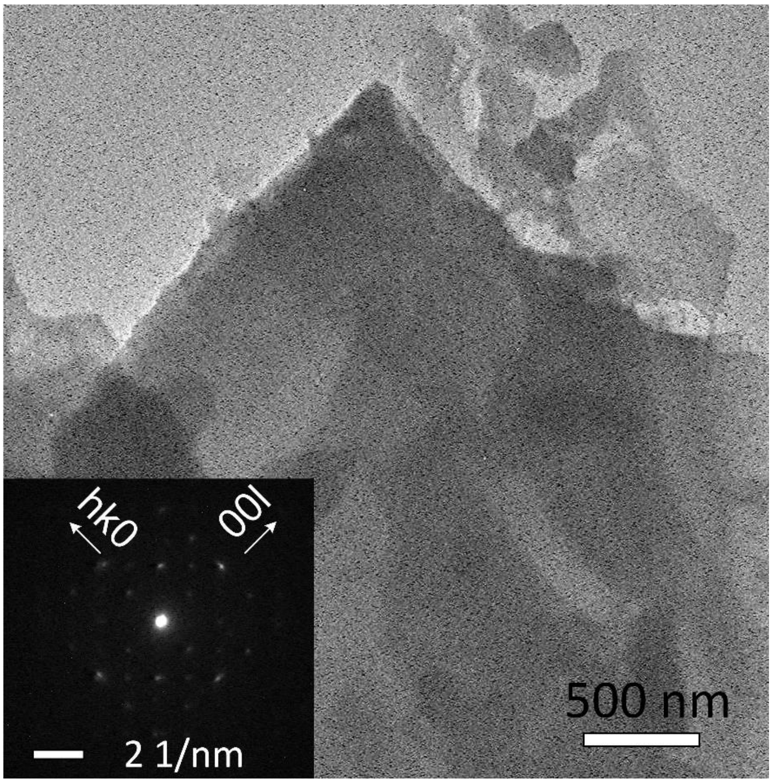

Figure S2. TEM image of a thin sheet. Inset: Electron diffraction pattern. Selected electron diffraction pattern confirm the $(BA)_2PbI_4$ crystallizes in the primitive centrosymmetric Pbca space group, as previously reported.[2]

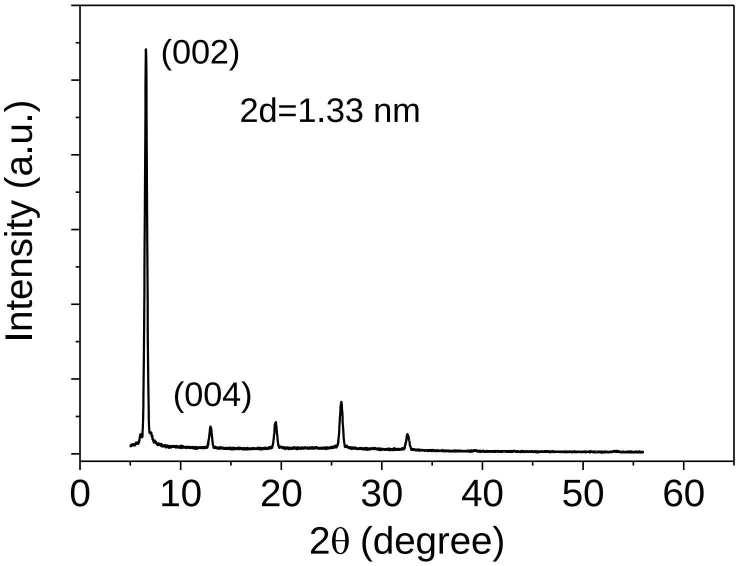

Figure S3. XRD pattern of the $(BA)_2PbI_4$ crystal. The well-defined XRD pattern further confirms good crystallinity of the acquired 2D perovskite. And the separation of the inorganic perovskite layers is estimated as 0.665 nm according to the (002) diffraction peak.

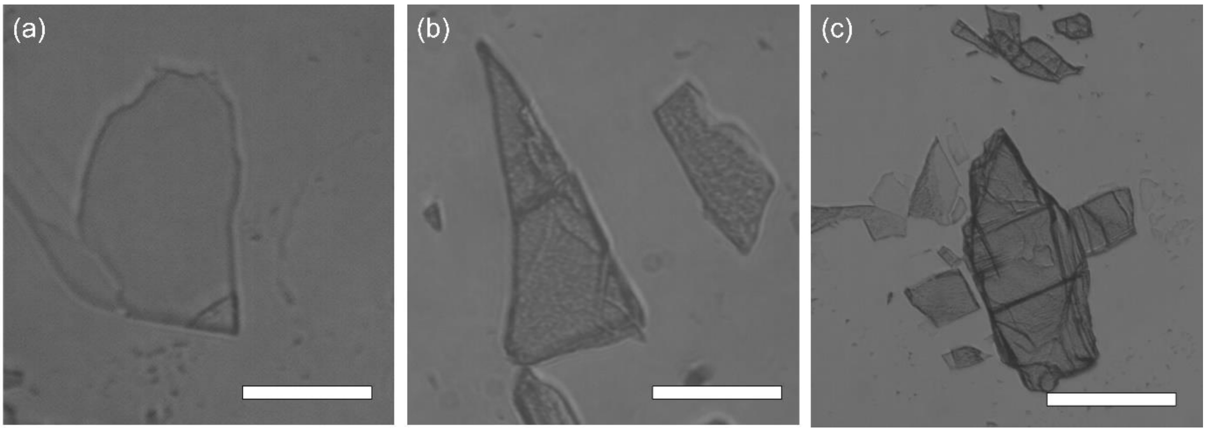

Figure S4. Three typical optical microscopic images of the cleaved $(BA)_2PbI_4$ platelets. Scale bar, 10 µm.

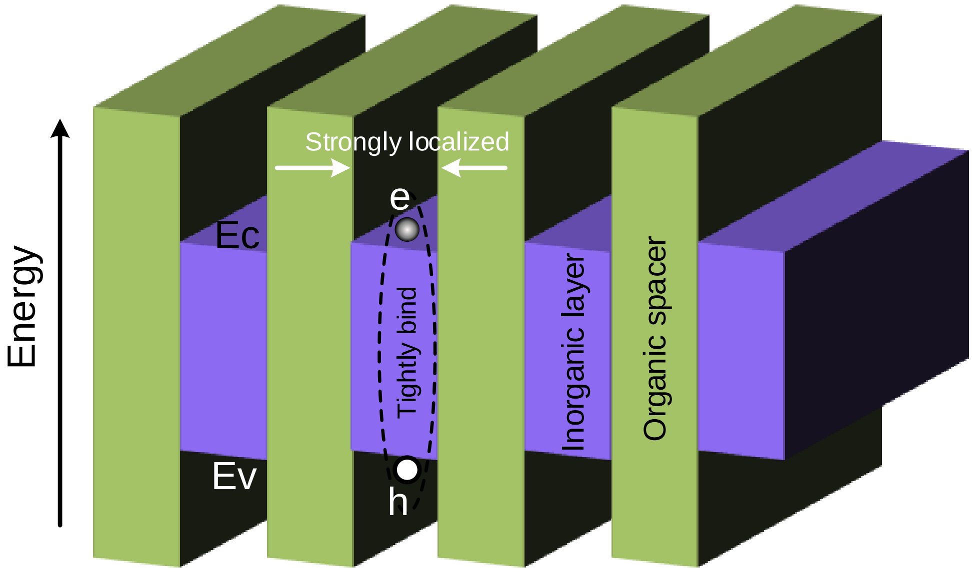

Figure S5. Illustration of exciton confined by the multi-quantum-wells (MQWs) structure. The inorganic perovskite layers are intercalated with insulating bulky butylammonium (BA) cations. The strong 2D quantum confinement has been confirmed in the MQWs electronic structure formed in these 2D perovskite structures.[3,4] The barrier and the well of these natural QWs have very different dielectric constants ($\varepsilon_{barrier}$ ~2.1; ε_{well} ~6.1).[5] Due to this high contrast in dielectric constants, the Coulomb interaction in the QW is strictly screened by the presence of the barrier: it is the well-known dielectric confinement effect.[6] Therefore, the electron-hole interaction within the exciton is very strong, resulting in huge oscillator strengths and very large exciton binding energies (of a few hundred of meV).[4] It has been demonstrated that the electronic coupling between the stacked quantum-wells is relatively low.[3]

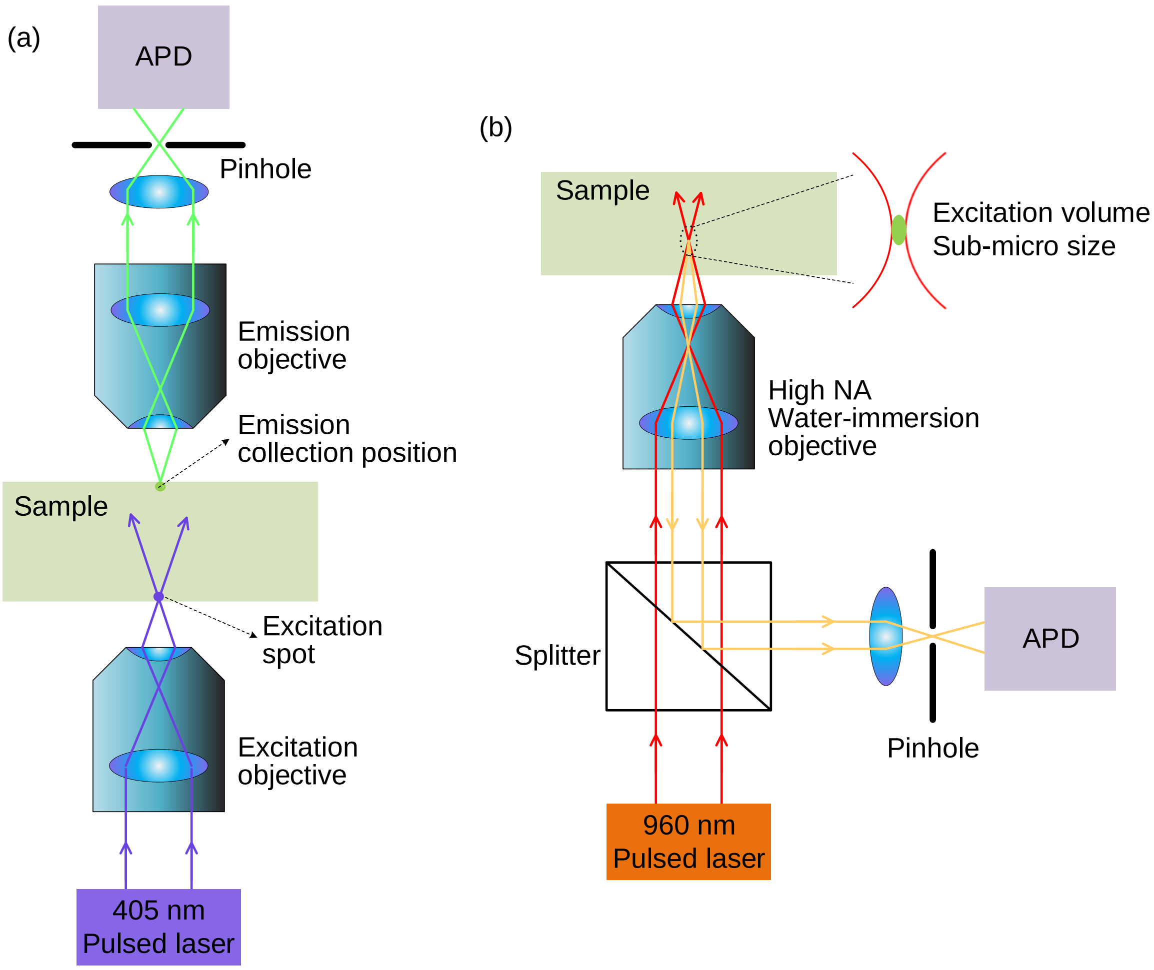

Figure S6. (a) A detailed scheme of the transmission geometry for PL/TRPL measurements. APD=avalanche photodiode. The excitation spot is focused on the surface of the 2D perovskite. While emission is collected on the surface of the other side. Based on this special design, the separation of excitation and emission spots in the z direction is controlled by the thickness of the perovskites. The two objectives are strictly aligned to eliminate the separation in x/y direction. (b) Scheme of the depth-resolved TPL measurements by two-photon laser scanning microscopy (TPLSM).[7] Two-photon absorption (TPA) is a third-order nonlinear optical process, thus the cross section of TPA is usually several orders of magnitude smaller than that of linear absorption at low light intensities. Both TPA and TPL are proportional to the square of the incident photon density. Therefore, TPL signal can be collected at a high temporal and spatial resolution by using an extremely temporally and spatially bound excitation volume produced by femtosecond laser pulses and a highly focused beam.

Table S1. A comparison of emission redshift from different reports.

Reference	Materials	Peak position		Shift	Note
Yamada, *Adv. Electron. Mater.* 2016, 2, 1500290.	$CH_3NH_3PbBr_3$ single crystals	2.316 eV 535.4 nm	2.26 eV 548.7 nm	56 meV 13.3 nm	The PL redshift during time variations.
Yamada, *Phys. Rev. Appl.* 2017, 7, 014001.	$CH_3NH_3PbBr_3$ single crystals	2.28 eV 543.9 nm	2.225 eV 557.3 nm	55 meV 13.4 nm	Depth dependent TPL.
Pazos-Outón, *Science* 2016, 351, 1430.	Thin lead iodide perovskite films	1.621 eV 765 nm	1.55 eV 800 nm	71 meV 35 nm	Spatial separation of emission and excitation spot.
Fang, *Nat. Commun.* 2017, 8, 14417	$CH_3NH_3PbBr_3$ single crystals	2.305 eV 538 nm	2.175 eV 570 nm	130 meV 32 nm	PL from reflection and transmission modes.
Wei, *Adv. Optical Mater.* 2017, 5, 1700809.	$CH_3NH_3PbBr_3$ films	2.313 eV 536 nm	2.255 eV 550 nm	58 meV 14 nm	Difference between PL and TPL.
Diab, *J. Phys. Chem. Lett.* 2017, 8, 2977.	$CH_3NH_3PbBr_3$ single crystals	2.23 eV 556.1 nm	2.19 eV 566.2 nm	40 meV 10.1 nm	Thickness dependent TPL.
This work	$(BA)_2PbI_4$ 2D crystals	2.377 eV 521.6 nm	2.305 eV 538 nm	72 meV 16.4 nm	Thickness dependent PL.

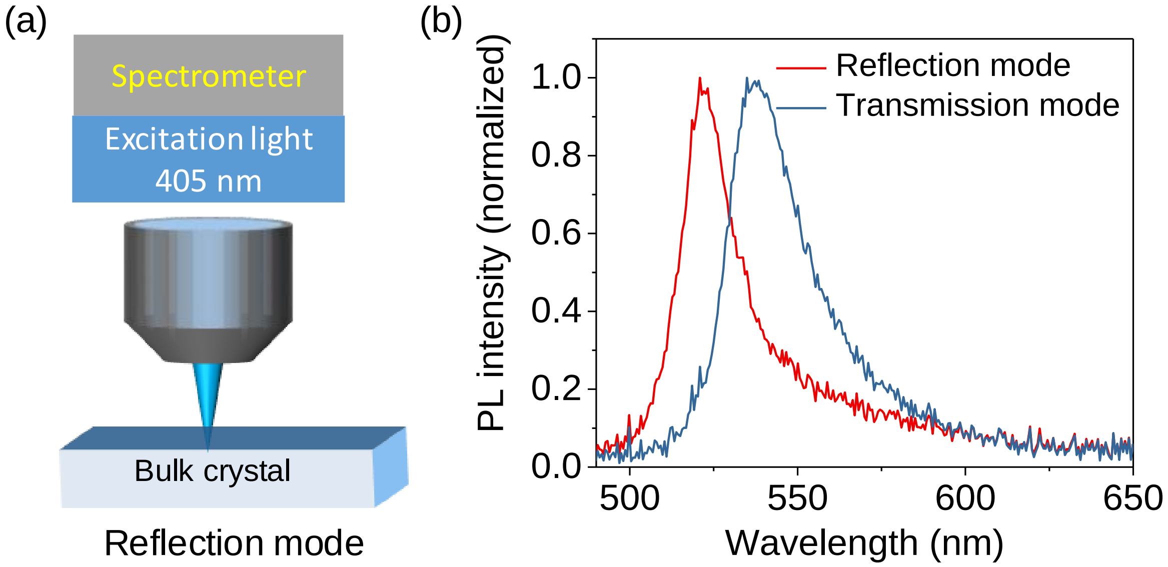

Figure S7. (a) The conventional reflection mode was used to measure the PL of the bulk crystal (thickness=396 µm). (b) Normalized PL spectra via reflection and transmission modes acquired from the same crystal. Compared to the PL by reflection mode, the PL from transmission mode exhibits a remarkable redshift due to photon recycling. The PL peak position of bulk crystal via reflection method is very close to the PL of the thinnest platelet via transmission method shown in Figure 2d.

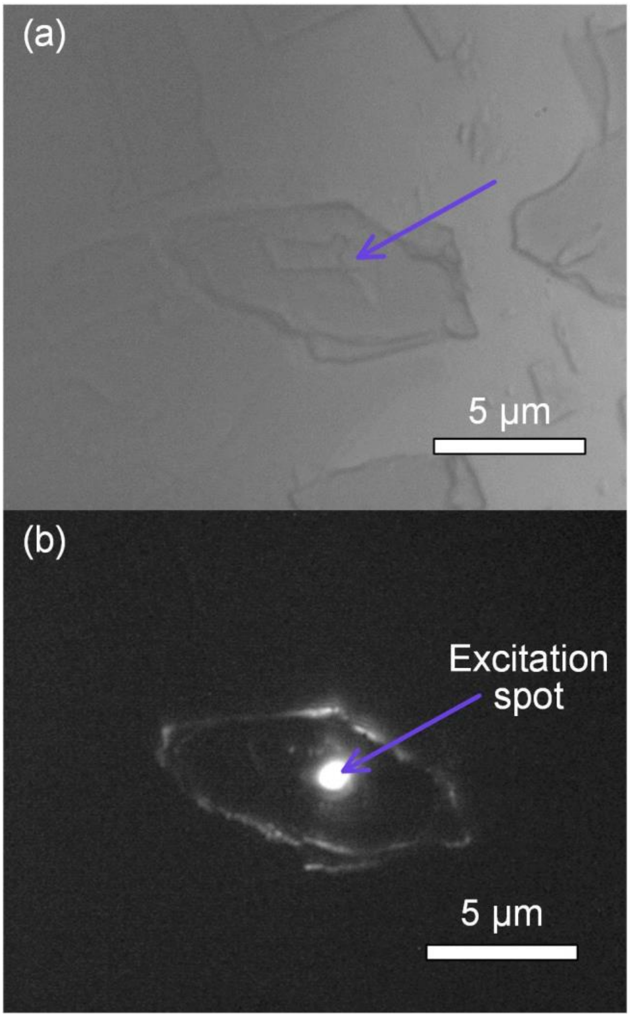

Figure S8. Observation of the waveguiding effect in 2D perovskite platelets. (a) Bright field optical microscopic image. (b) Dark field optical microscopic image with a 405 nm excitation. The image was recorded by a CCD camera with a 450 nm long-pass filter. The bright edge indicates waveguiding effect of the fluorescent photons, which directly verifies the long photon transport distance within the perovskites. However, the visualization of long-distance carrier diffusion is usually realized by an indirect optical measurements,[8-10] thus doubtful.

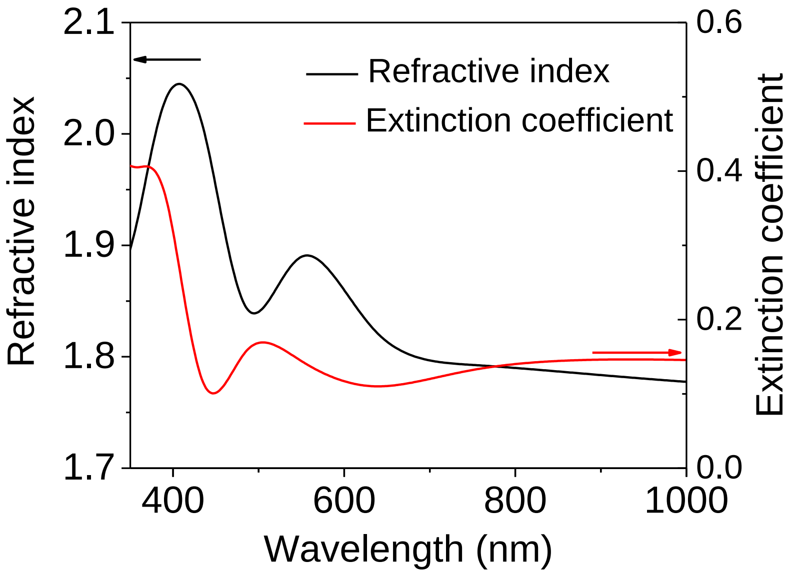

Figure S9. Refractive index and extinction coefficient of the $(BA)_2PbI_4$ crystal acquired by spectroscopic ellipsometry (J.A. Woollam). The large refractive index ensure the fluorescent photons confined in the perovskites with narrow escape cone, which facilitates the photon recycling.

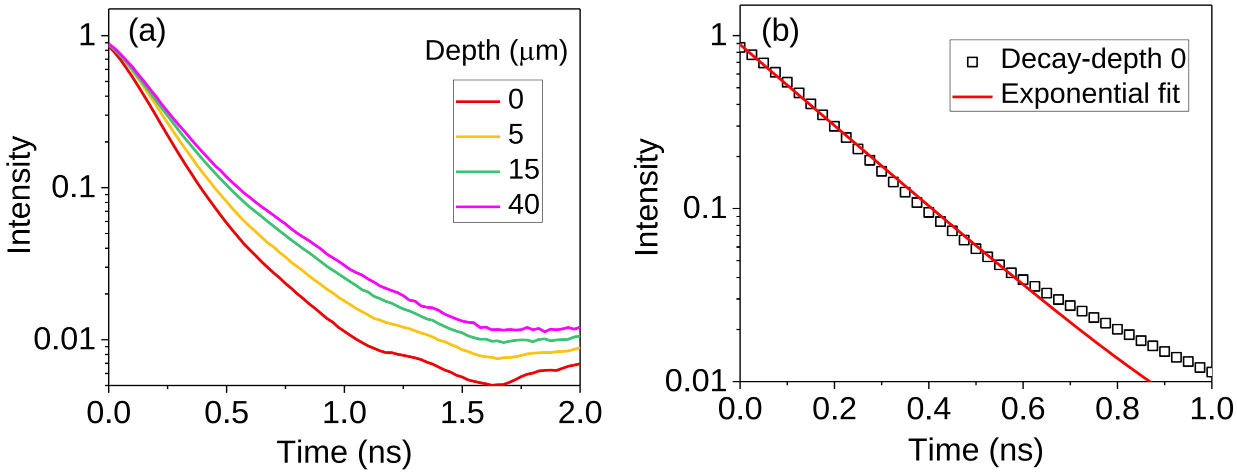

Figure S10. (a) TPL decay traces of 2D perovskite crystal at different depths. (b) Exponential fit of a typical TPL decay curve.

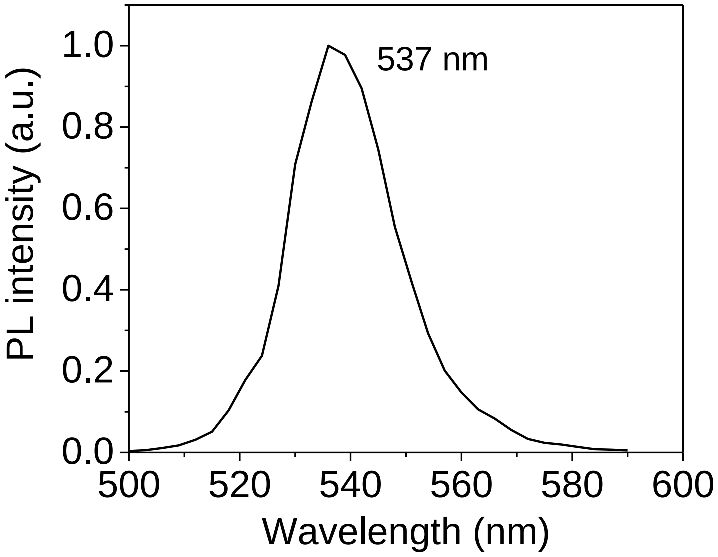

Figure S11. PL spectrum of the $MAPbBr_3$ crystal excited at 488 nm. The PL was measured by a reflection mode on a confocal system (Figure S6a) and the excitation beam was focused on the surface of the crystal. The PL peak appears at 537 nm, indicating no obvious redshift.

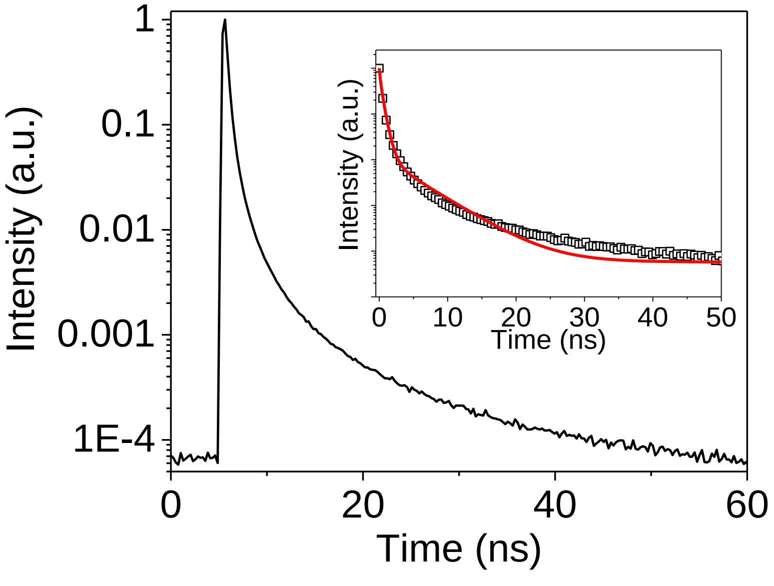

Figure S12. PL decay curve of the $MAPbBr_3$ crystal (excitation: 470 nm and emission: 537 nm). Inset: A stretched-exponential ($Aexp(-t/\tau_1) + Bexp(-(t/\tau_2)^{\beta})$) fit of the PL decay trace. $A = 0.012$, $B = 0.994$ τ_1=4.65 ns, $\tau_2 = 0.319$ and β=0.8 are acquired. The former exponential term in equation represents the relaxation of free or extended states towards localized states, whereas the latter stretched-exponential term accounts for the communication between the localized states. The effective lifetime (τ_{eff}) is defined as $\frac{A\tau_1+B\tau_2}{A+B}$. Thus, carrier diffusion length L_D is estimated to be no longer than 1.055 μm based on $\mathrm{L_D} = \sqrt{\mathrm{D}\tau_{eff}}$, where $\tau_{eff} = 0.371\ ns$ and *D* is the carrier diffusion coefficient[8]. The reported *D* is normally in the range of 0.03 to 3 $\mathrm{cm^2s^{-1}}$. [11,12] An upper limitation of diffusion length is acquired by assuming *D*=3 $\mathrm{cm^2s^{-1}}$.

Interestingly, as shown in Figure 7d, if the TRPL is measured by a transmission mode, a much longer lifetime is acquired due to the photon recycling, resulting in an overestimation of carrier diffusion length. On the other hand, the evidently extended PL lifetime confirms the collected PL at the rear is not from simple filtering effect. Moreover, it is worth noting the PL peak position by transmission mode (Figure 7c) substantially redshift compared to the PL acquired by reflection mode (Figure S11). Therefore, in both 2D and 3D perovskites, the redshifted peak position and extended lifetime are the two primary features for the emission detected after energy transport.

Note S1. Interpretation on the relationship between peak position ($\mathrm{E}(\boldsymbol{l})$) and depth ($\boldsymbol{l}$)

The emission photon energy at depth of l is described as:

$$E(l)\ = E_{min} + E_0\exp\left(-\frac{l}{L_0}\right), \qquad \text{(E-S1)}$$

where $E_{min} + E_0 = E_{max}$ and E_{min} are the photon energies of the initial emission without redshift and the emission through a depth $l \to \infty$, respectively. This relationship is acquired by approximating that the emission peak position is modified according to

$$E(l) \to E_{max} - E_0[1 - (\eta_{PR})^{N_{PR}}], \qquad \text{(E-S2)}$$

when photon recycling occurs N_{PR} circles, $\eta_{PR} = \phi_{PL}\eta_\alpha$ is the fraction of photons contributing to one circle of photon recycling and $N_{PR} = \frac{l}{\sqrt{{L_\alpha}^2+{L_D}^2}}$.

$$E(l) = E_{max} - E_0 + E_0(\eta_{PR})^{N_{PR}}$$

$$= E_{min} + E_0\exp(N_{PR} ln\eta_{PR})$$

$$= E_{min} + E_0\exp\left(\frac{l}{\sqrt{{L_\alpha}^2 + {L_D}^2}} ln\eta_{PR}\right)$$

$$= E_{min} + E_0\exp\left(-\frac{l}{L_0}\right)$$

$\frac{\sqrt{{L_\alpha}^2+{L_D}^2}}{-ln\eta_{PR}}$ is written as L_0

Obviously, the equation E-S1 is an approximation to fit the experimental results, analogous to the equation (5) developed by Yamada[13]. When the depth (l) increases, the energy shift increases, resulting in the continuous redshift of emission. However, photon recycling is essentially caused by the overlap between absorption and emission spectra. As emission further redshifts, the overlap decreases, so as the photon recycling decreases and finally terminates. It implies that both the first and the second derivatives of $E(l)$ should be negative. When the depth is large enough, the overlap between absorption and emission is negligible, photon recycling disappears. Thus, $E(l)$ should be a bounded function. Equation E-S1 matches all the requirements and successfully fits the experimental results, implying it is a suitable approximation.

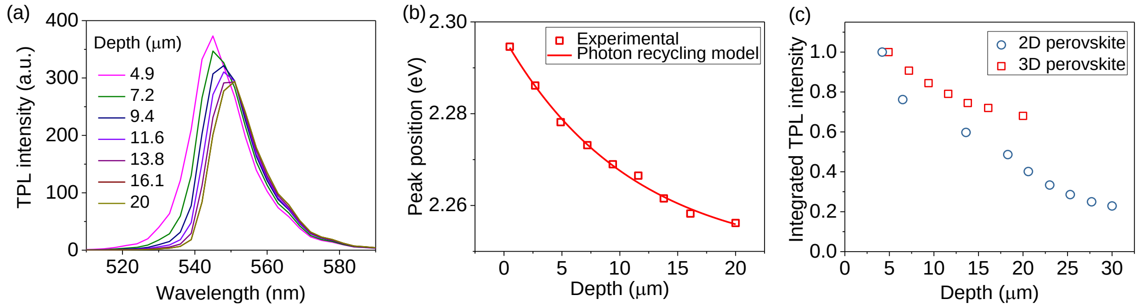

Figure S13. (a) TPL spectra acquired from a 3D $MAPbBr_3$ bulk crystal at different depths. As depth increases, PL peak gradually redshifts with decreased intensity. (b) Depth resolved TPL peak positions of 3D $MAPbBr_3$ crystal fitted by an exponential function (E-S1). (c) A comparison of the depth-resolved TPL intensities of 2D perovskite (circles) and 3D $MAPbBr_3$ crystal (squares). The two relationships are very close.

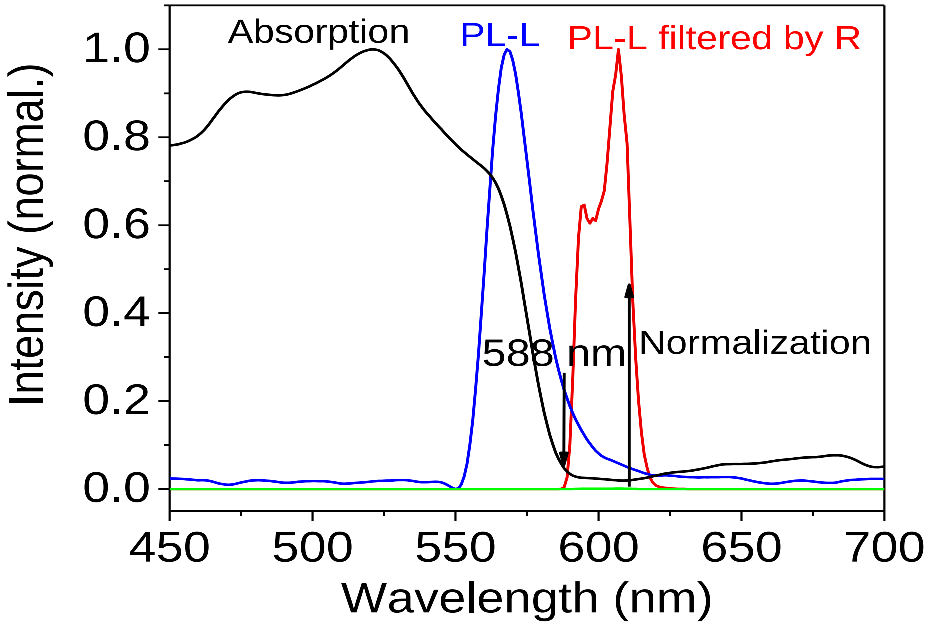

Figure S14. Absorption spectrum of a $MAPbBr_3$ crystal (black line), and a comparison of PL before and after filtering by the R crystal (See scheme in Figure 6b). PL-L is the experimental PL spectrum of L crystal (blue line) and PL-L filter by R is calculated by Beer–Lambert model (green line: before normalization; red line: after normalization).

Supposing the PL at the rear is purely produced by direct carrier diffusion without photon recycling, the fluorescent photons emit from L crystal cannot re-excite the R crystal, consequently, fluorescence of L is simply filtered by R crystal. As shown in Figure S14, due to the strong absorption at wavelength shorter than 588 nm, all the fluorescent photons from L crystal at wavelength shorter than 588 nm are sharply removed after filtering. And the PL intensity tremendously quenches (green line). After normalization (red line), the slight noises in absorption and PL are largely amplified, resulting in the concave in the calculated PL spectrum.

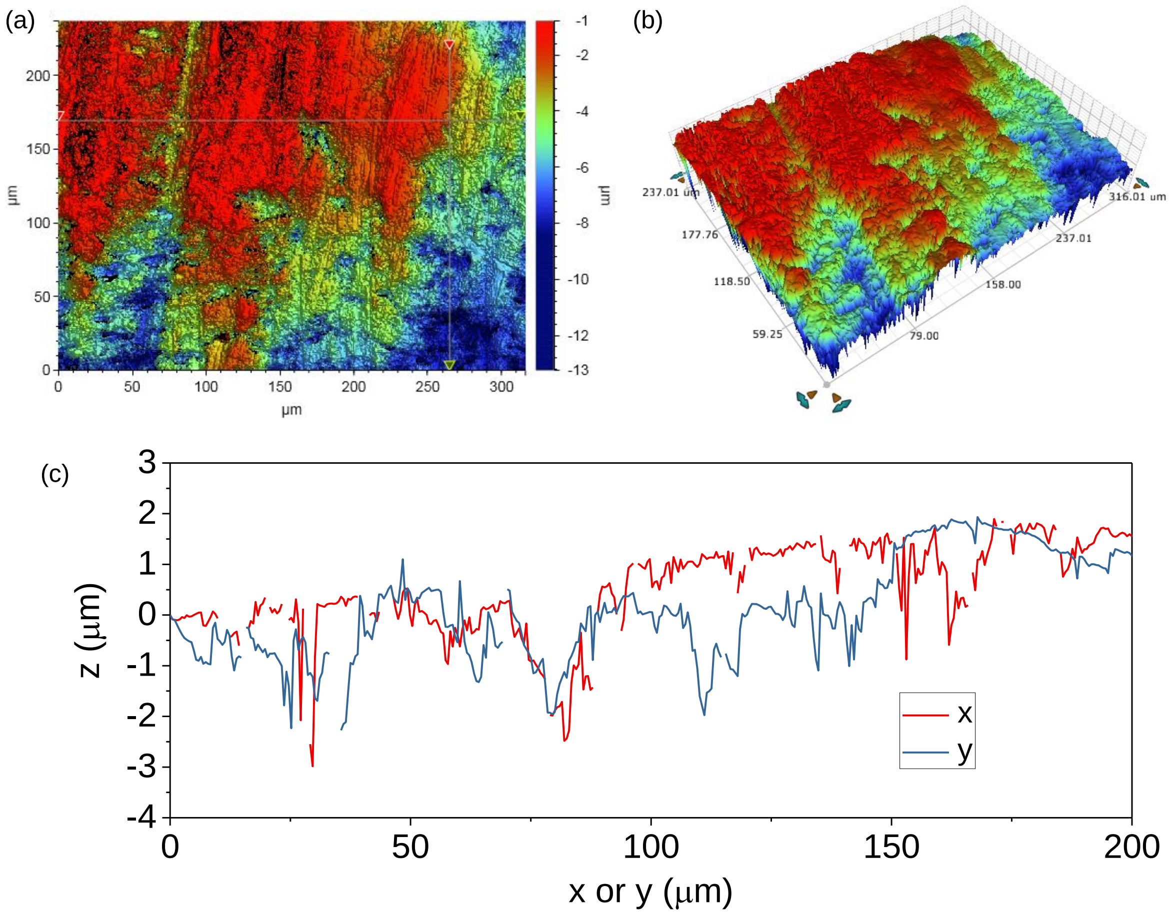

Figure S15. (a,b) A typical topographic profile image of the cleavage section measured with an optical profiler (Bruker ContourGT InMotion). (c) Corresponding height profiles. The rough surface exhibits fluctuations of ca. 3 µm.

Note S2. Model for pure carrier diffusion

The diffusion of photogenerated carriers is mainly driven by concentration gradient (∇n), thus the diffusion fluence is $-D \cdot \nabla n$. The accumulation rate of carriers at specific point per unit time is the differential of fluence, $D \cdot \nabla^2 n$. At steady-state after pulse excitation, carrier accumulation rate equals the disappearance by recombination,

$$\mathrm{D} \cdot \nabla^2 \mathrm{n} = n/\tau. \quad \text{(E-S3)}$$

For one dimensional diffusion, the solution for the above equation can be written as

$$n = \mathrm{A}\exp\left(-\frac{z}{\mathrm{L_D}}\right) + \mathrm{B}\exp\left(\frac{z}{\mathrm{L_D}}\right), \quad \text{(E-S4)}$$

where $L_D = \sqrt{\mathrm{D}\tau_{\mathrm{eff}}}$. Considering the boundary conditions, $n = 0$ at $z = \mathrm{d}$ and $n = \mathrm{n}_0$ at $z = 0$ (excitation position).

$$\begin{cases} A = \mathrm{n}_0 \frac{\exp(d/\mathrm{L_D})}{\exp(d/\mathrm{L_D}) - \exp(-d/\mathrm{L_D})} \\ B = \mathrm{n}_0 \frac{\exp(-d/\mathrm{L_D})}{\exp(d/\mathrm{L_D}) - \exp(-d/\mathrm{L_D})} \end{cases} \qquad \text{(E-S5)}$$

The distribution of photogenerated carriers along z direction is plotted in Figure S16a. As excitation depth increases, the carrier distributions are very similar, which is essentially dependent on L_D. In this pure carrier diffusion model, when excitation depth is larger than 10 μm, the carrier density at the surface of (-5 to 0 μm) is extremely low. The integrated carrier concentration at -5 to 0 μm is plotted versus excitation depth in Figure S16c. If only recombination of carriers at this defined surface can be detected by the spectrometer, the PL intensity rapidly decreases as excitation depth increases. When excitation depth is larger than 10 μm, the PL intensity becomes nearly zero. But the experimental results (Figure S13) apparently disagree with this tendency.

In terms of the decay lifetime, the carrier generated by pulsed laser is described by one-dimensional continuity equation,

$$\frac{\partial \mathrm{n(z,t)}}{\partial \mathrm{t}} = D\frac{\partial^2 n}{\partial z^2} - \frac{\mathrm{n}}{\tau}. \qquad \text{(E-S6)}$$

Assuming, at $t = 0$, the carriers concentrate in the neighbourhood $z \in (-\delta, \delta)$ of excitation spot (*z*=0), the solution becomes

$$n(t, z) = \frac{N_i}{\sqrt{4\pi Dt}} \exp[-(\frac{z^2}{4Dt} + \frac{t}{\tau})], \qquad \text{(E-S7)}$$

Where N_i is the photo-generated carrier density at $t = 0$. By assuming $\tau = 0.37$ ns and $D = 3\ \mathrm{cm^2 s^{-1}}$ (Figure S12), the simulated decay curves of carrier concentration at different distances (*z*) are plotted in Figure S17. There is a time delay on the rising side as *z* increases, whereas, the decay traces are very similar. Hu *et al* have observed a rising time of ∼1.5 ns corresponding to the delay time of drifted carriers over the distance from the excitation to the detection positions[10]. Whereas, for pure photon recycling, photon propagation and absorption is much faster than radiative recombination, the time delay on the rising side is negligible[12]. A comparison of TRPL produced by pure carrier diffusion and photon recycling is summarized in Table S2. In this work, TPL of 2D perovskites exhibits decay lifetime increases as depth increases without time delay on the rising side (Figure 4d and Figure S10). And the PL lifetime of 3D crystal by the transmission model (Figure 7d) is remarkably longer than that obtained through a reflection model (Figure S13). Thence PL lifetime results again disagree with the pure carrier diffusion model.

From the aspect of photon energy, no quantitative relationship is available yet. Since hot carrier cooling is much faster than carrier diffusion. The cooling process by coupling with acoustic phonons and longitudinal optical phonons normally complete before diffusion, indicating the peak should hardly change with diffusion distance for the ideal case. However, the conduction band bottom has an intrinsic broadening, such as fine structure due to spin-orbit coupling,[14,15] as well as bandtails caused by structural disorders. Due to the long-lived carrier-carrier interactions,[16,17] carrier-lattice coupling, and structural inhomogeneity, the excited carriers may lose a small amount of energy after diffusion, resulting in redshift of photon energy.

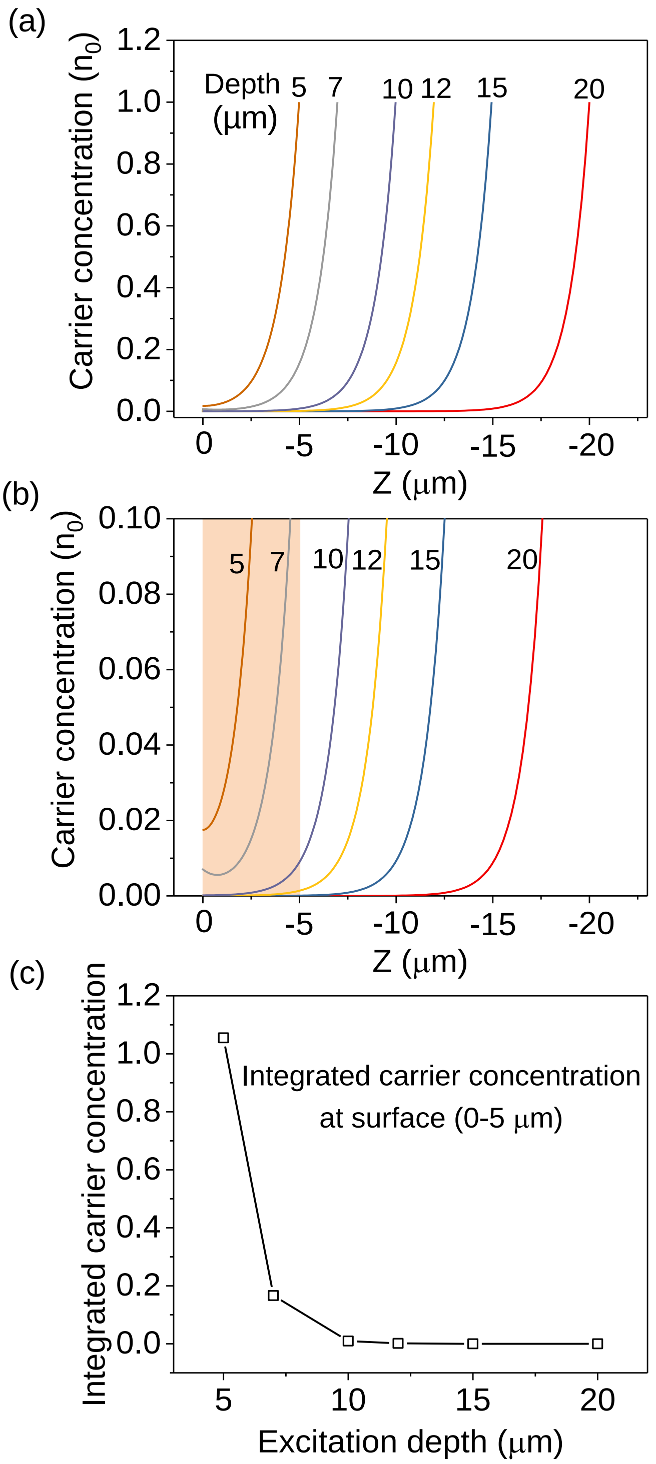

Figure S16. (a) Carrier distributions calculated by equation E-S4 by setting $L_D = 1.055\ \mu m$, (b) An enlargement of (a). (c) Integrated carrier concentration at -5 to 0 μm versus excitation depth.

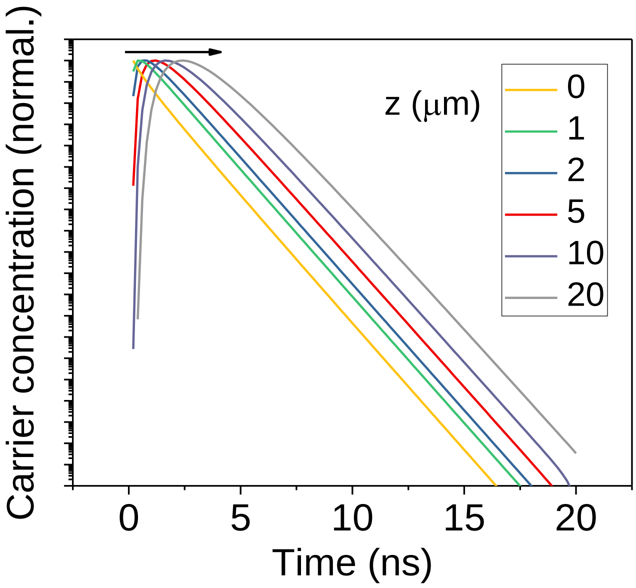

Figure S17. Simulated decay of carrier concentration at different distances (z) according to equation E-S7.

Table S2. A comparison of TRPL produced by pure carrier diffusion and photon recycling.

	Intensity rising side	**Intensity decay side**
Carrier diffusion	Time delay with distance	Independent with distance
Photon recycling	Scarcely change with distance	Prolonged with distance

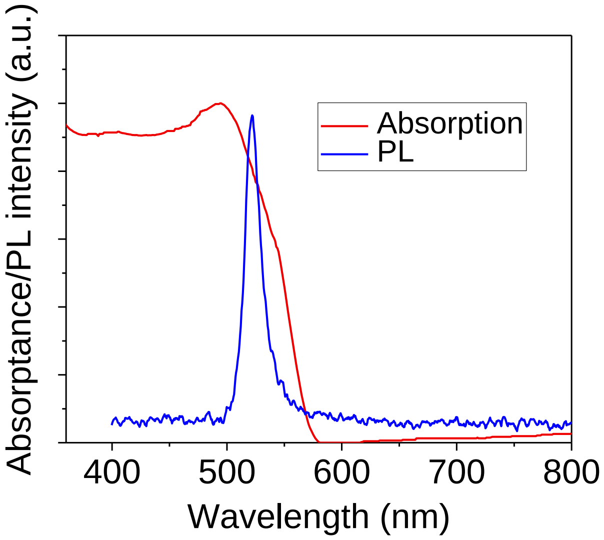

Figure S18. A comparison of normalized absorption and PL spectra.

Note S3. More justifications

(1) $MAPbI_3$ is a very important member of perovskite family. However, due to following reasons, we mainly focus on $MAPbBr_3$ in this work.

Firstly, the iodine based 2D material is more similar to $MAPbBr_3$ than $MAPbI_3$. The bandgap of $MAPbI_3$ is 1.59 eV, carrier lifetime could be as long as tens of nanoseconds or even longer, while the carrier diffusion coefficient is $D=0.0054$ cm^2/s. Secondly, 2D perovskite is the starting point of our design. However, it is difficult to find a reference 2D perovskite similar to $MAPbI_3$.

(2) Difference between 2D $(BA)_2PbI_4$ and 3D $MAPbBr_3$.

Although, the photon recycling related parameters of $MAPbBr_3$ and $(BA)_2PbI_4$ crystals are very similar, such as, bandgap, absorption efficiency, internal PL QY, refractive index, and intrinsic stokes-shift, there are still some differences in carrier dynamics. The emission of 3D $MAPbBr_3$ originates from free carrier recombination, while, the emission of 2D $(BA)_2PbI_4$ is dominated by excitonic recombination. The onset for excitonic and free carrier absorption has a different dependence on energy. Excitons have a much longer absorption tail due to the Lorentzian shape of the absorption edge. However, for all the numerical analysis, absorption coefficient is used from the experimental result, thus the real situation including this kind of difference has been taken into account.

(3) Difference between one-photon and two-photon excitation.

For one-photon-excitation, the carriers usually are generated along surface, less than 200 nm in depth, due to the limited absorption depth. Whereas, for two-photon-excitation, the carriers are generated in an ellipsoidal volume (size<100) nm due to the nonlinear effect and a threshold. The carrier diffusion distance is about 1000 nm. The approximate resolution of the depth resolved two-photon PL setup in z-direction is ~500 nm. Thus, when the depths/thicknesses are the same, the difference between 1P vs 2P excitation cannot be resolved.

(4) More explanations on Figure 5.

Firstly, as schemed in Figure 5b, a lateral offset of 15 µm suggest the distance changes from 396 to 396.28 um. The additional distance is 0.28 µm rather than 15 µm. Secondly, even if the additional distance is 15 µm. The transport distance changes from 396 to 411 µm. According to the relationship shown in Figure 3c, the PL peak position changes nonlinearly with the transport distance. When the distance is larger than 300 um, the PL peak almost keeps constant with distance. The process is calculated by the following equation (See details in Note S1, SI),

$$E(l) = E_{min} + E_0 \exp\left(-\frac{l}{L_0}\right)$$

$E(l)$ is almost the same for $l = 396$ and l =411 µm, since $E_0 \exp\left(-\frac{l}{L_0}\right) \approx 0$ for both $l = 396$ and l =411 µm. Thus, we intentionally choose a thick bulk for this experiment.

We stress that the change from 396 to 411 µm is definitely different from that responsible for the change from 0 to 15 µm. $E(l) = E_{min}$ for both l =396 and 411 um. Whereas $E(l) = E_{min} + E_0$ and $E(l) \approx E_{min} + \frac{E_0}{e}$ for l=0 and 15 um, respectively. For photon transport, the distance changes from 396 to 411 µm, there will be NO more additional redshift caused by photon recycling. Whereas the distance allowing for carrier transport changes from 0 to 15 um. Therefore, in this design, the dependence of photon recycling on peak position is negligible, so that we can solely check the contribution from carrier diffusion. If carrier diffusion has a significant contribution, both the PL peak position and TRPL should remarkably change. However, as shown in Figure 5c and d, no discernible changes can be observed in the PL peak position and TRPL at different separations (0-15 µm), indicating the carrier diffusion, when it indeed exists in general perovskites, scarcely contributes to the PL collected separated from the excitation spot.

(5) Influence of photon recycling on LED efficiency.

Only when the out-coupling probability (η_{esc}) is very low, the photon recycling is strong. In other words, the strong photon recycling normally means low external efficiency (η_{ext}). For an internal yield of 70%, the external yield is as low as 15% in a planar film due to the low light out-coupling.[18]

Assuming two ideal cases with the same out-coupling probabilities, case one is pure carrier diffusion and case two is pure photon recycling. For case one, all the carriers recombine after diffusion with only one single out-coupling event, $\eta_{ext-1} = \eta_{IN} \cdot \eta_{esc}$. For case two, multiple recycling events would allow multiple emission events, each with an out-coupling probability to leave, $\eta_{ext-2} = \frac{\eta_{IN} \cdot \eta_{esc}}{1-\eta_{IN}+\eta_{IN} \cdot \eta_{esc}}$.[18] It is evident $1 - \eta_{IN} + \eta_{IN} \cdot \eta_{esc} < 1$, thus, $\eta_{ext-2} > \eta_{ext-1}$.

(6) Surface interactions with moisture and/or oxygen

Our samples are stored and treated in a glove box with inert atmosphere, while the measurements are done in air (low humidity <50% at 21 °C). To avoid the structural degradation and minimize the surface interactions, the samples were freshly prepared for all the measurements. And all the measurements are conducted in a timely fashion. Moreover, the sample in our measurements are relatively thick compared to the surface. The thinnest one is 51 nm, which contains multiple atomic layers. From both structural characterization and PL measurements, no evident degradation is observed, indicating the interactions with moisture and/or oxygen is weak. Moreover, we have very important results from depth-resolved TPL. For TPL measurements, the photocarriers are directly generated in the interior region, where surface effect is expected to be extremely low. Figure 4 shows the similar dependence of PL peak with film thickness and TPL peak with excitation depth, indicating the PL is also less affected by surface effect.

(7) Photostability of the 2D $(BA)_2PbI_4$ crystal.

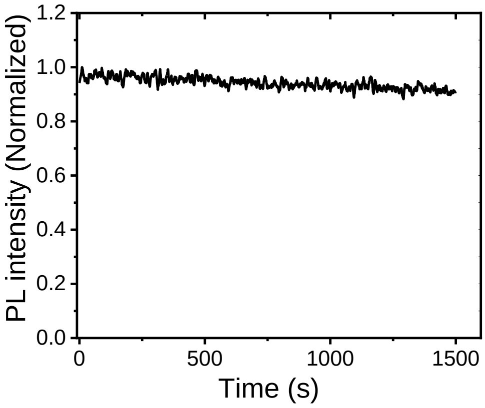

Figure S19. PL intensity recorded during continuous irradiation (excitation density: 0.5 $\mu J/cm^2$), showing no noticeable photobleaching effect. Note for other results shown in the manuscript, the PL tests on a single sample were typically completed in 15 minutes. And the excitation power density used for PL measurements was 0.1 $\mu J/cm^2$. Therefore our conclusion is basically unaffected by the photobleaching effect.

SI References

1. Fang, Y., Wei, H., Dong, Q. & Huang, J. Quantification of re-absorption and re-emission processes to determine photon recycling efficiency in perovskite single crystals. *Nat. Commun.* **8**, 14417 (2017).
2. Stoumpos, C. C. *et al.* Ruddlesden−Popper hybrid lead iodide perovskite 2D homologous semiconductors. *Chem. Mater.* **28**, 2852−2867 (2016).
3. Xing, G. *et al.* Transcending the slow bimolecular recombination in lead-halide perovskites for electroluminescence. *Nat. Commun.* **8**, 14558 (2017).
4. Gauthron, K. *et al.* Optical spectroscopy of two-dimensional layered $(C_6H_5C_2H_4\text{-}NH_3)_2$-$PbI_4$ perovskite. *Opt. Express* **18**, 5912–5919 (2010).
5. Ishihara, T., Takahashi, J. & Goto, T. Optical properties due to electronic transitions in two dimensional semiconductors $(C_nH_{2n+1}NH_3)_2PbI_4$," *Phys. Rev. B* **42**, 11099–11107 (1990).
6. Kumagai, M. & Takagahara, T. Excitonic and nonlinear optical properties of dielectric quantum-well structures. *Phys. Rev. B* **40**, 12359–12381 (1989).

7. Chen, W. *et al.* Nanoscale characterization of carrier dynamic and surface passivation in InGaN/GaN multiple quantum wells on GaN nanorods. *ACS Appl. Mater. Interfaces* **8**, 31887−31893 (2016).
8. deQuilettes, D. W. *et al.* Tracking photoexcited carriers in hybrid perovskite semiconductors: trap-dominated spatial heterogeneity and diffusion. *ACS Nano* **11**, 11488−11496 (2017).
9. Tian, W., Zhao, C., Leng, J., Cui, R. & Jin, S. Visualizing carrier diffusion in individual single-crystal organolead halide perovskite nanowires and nanoplatelets. *J. Am. Chem. Soc.* **137**, 12458−12461 (2015).
10. Hu, X. *et al.* Visualizing carrier transport in metal halide perovskite nanoplates via electric field modulated photoluminescence imaging. *Nano Lett.* **18**, 3024−3031 (2018).
11. Yun, J. S. *et al.* Benefit of grain boundaries in organic−inorganic halide planar perovskite solar cells. *J. Phys. Chem. Lett.* **6**, 875−880 (2015).
12. Yang, Y., Yan, Y., Yang, M., Choi, S., Zhu, K., Luther, J. M. & Beard, M. C. Low surface recombination velocity in solution-grown $CH_3NH_3PbBr_3$ perovskite single crystal. *Nat. Commun.* **6**, 7961 (2015)
13. X. Wu, *et al.* Trap states in lead iodide perovskites, *J. Am. Chem. Soc.* **137**, 2089−2096 (2015).
14. Braly I. L. *et al.* Hybrid perovskite films approaching the radiative limit with over 90% photoluminescence quantum efficiency. *Nat. Photon.* **12**, 355–361 (2018).
15. Price, M. B. *et al.* Hot-carrier cooling and photoinduced refractive index changes in organic-inorganic lead halide perovskites. *Nat. Commun.* **6**, 8420 (2015).
16. Booker, E. P. *et al.* Formation of long-lived color centers for broadband visible light emission in low-dimensional layered perovskites. *J. Am. Chem. Soc.* **139**, 18632−18639 (2017).
17. Fu, J. *et al.* Hot carrier cooling mechanisms in halide perovskites. *Nat. Commun.* **8**, 1300 (2017).
18. Richter, J. M. *et al.* Enhancing photoluminescence yields in lead halide perovskites by photon recycling and light out-coupling. *Nat. Commun.* **7**, 13941 (2016).